dynamics

MDPI

Article

Dynamic Analysis of a Chaotic Financial System with Reflexive Market Sentiment

Chamalka Dharmasiri [1] and Upeksha Perera [2,*]

[1] Department of Mathematics, University of Peradeniya, Peradeniya 20400, Sri Lanka; chamalka.dharmasiri@gmail.com
[2] Department of Mathematics, University of Kelaniya, Dalugama, Kelaniya 11600, Sri Lanka
* Correspondence: upeksha@kln.ac.lk

Abstract

We develop a four-dimensional nonlinear model of a reflexive financial system by extending the Xin–Zhang system with a self-reinforcing sentiment channel. The model comprises four interacting variables—interest rate, investment demand, price index, and market confidence—and incorporates reflexivity to capture feedback between economic fundamentals and investor sentiment. A Lyapunov function shows that the system is well-posed and dissipative, ensuring bounded trajectories. We then analyse the dynamics using standard nonlinear-dynamics tools. Reflexive confidence sustains chaotic motion, inhibits convergence to equilibria, and produces irregular, aperiodic bifurcation patterns; sentiment-driven feedback destabilises a dissipative macroeconomic model and sustains volatility, as evidenced by a positive largest Lyapunov exponent and Kolmogorov–Sinai entropy greater than zero. Using U.S. monthly consumer sentiment and the S&P 500, we observe co-movement, a medium-horizon lead of sentiment, and a nonlinear persistence map $w_{t+1} = f(w_t)$—stylised facts consistent with the model's self-reinforcing confidence channel.

Keywords: chaotic financial system; reflexivity; market sentiment; Lyapunov exponents; nonlinear dynamics; fractal attractors; equilibrium stability; behavioural macroeconomics

PACS: 05.45.-a; 05.45.Gg; 89.65.Gh

MSC: 37D45; 91B74; 37G15; 93D20

JEL Classification: C63; E44; D84

Academic Editor: Christos Volos

Received: 26 August 2025
Revised: 18 October 2025
Accepted: 23 October 2025
Published: 10 November 2025

Citation: Dharmasiri, C.; Perera, U. Dynamic Analysis of a Chaotic Financial System with Reflexive Market Sentiment. *Dynamics* **2025**, *5*, 47. https://doi.org/10.3390/dynamics5040047

1. Introduction

Chaotic systems are nonlinear dynamical systems that exhibit extreme sensitivity to initial conditions, leading to complex and unpredictable long-term behaviour. Such systems arise in diverse fields, including weather prediction, engineering, biology, and finance. In economic contexts, understanding chaotic dynamics is vital for analysing instability, improving forecasting, and guiding risk management strategies. This has motivated a substantial literature on nonlinear and chaotic dynamics in economics and finance [1–3]. In continuous-time, low-dimensional ODE models of financial variables (interest rate, investment, prices) already display rich nonlinear behaviour. For broader context on chaos in economic models—including discrete time and implicitly defined frameworks—see [4–6].

Market confidence is crucial in financial systems as it affects how people invest and spend. It stands for the confidence that consumers and investors have in the state of the

economy. More investment and economic growth happen when confidence is high, which is frequently the result of low interest rates. Conversely, low confidence, which can result from high interest rates or economic uncertainty, may reduce investment and increase unemployment. Consumer spending is influenced by spending confidence, which is linked to investment confidence. Understanding and modelling these factors helps create better strategies to strengthen market stability and resilience.

The widely studied 3D Ma–Chen system provides a classical basis for modelling macroeconomic instability through the interaction of interest rate (x), investment demand (y), and price index (z) [7,8]. 4D Xin–Zhang system extends this framework by introducing market confidence (w) as a fourth state variable [9], but in the context of a fractional-order formulation. Their system captures the influence of market sentiment on macroeconomic variables through the coupling terms m_1, m_2, and m_3, but does not account for the self-reinforcing nature of confidence.

The 4D market confidence system is formulated as follows:

$$\begin{aligned} \dot{x} &= z + (y - a)x + m_1 w, \\ \dot{y} &= 1 - by - x^2 + m_2 w, \\ \dot{z} &= -x - cz + m_3 w, \\ \dot{w} &= -xyz\,. \end{aligned} \tag{1}$$

Here, a, b, and c are non-negative constants representing the amount saved, cost per investment, and demand elasticity, respectively. The parameters m_1, m_2, and m_3 quantify the effect of confidence on the system.

The concept of reflexivity in financial markets, originally proposed by George Soros [10], emphasises the bidirectional relationship between market participants' perceptions and actual market outcomes. According to this theory, investor beliefs influence economic fundamentals through actions such as buying, selling, or investing, which in turn shape those same beliefs—a self-reinforcing feedback loop. This contrasts with traditional economic models that assume markets operate under rational expectations and equilibrium conditions. Reflexivity captures the behavioural and psychological mechanisms by which sentiment amplifies booms or accelerates downturns, and is particularly relevant during periods of uncertainty and volatility. Despite its conceptual importance, reflexivity has remained difficult to formalise mathematically, especially in the context of nonlinear dynamical systems.

Formalizations of reflexivity and self-exciting feedback in markets include Hawkes-process reflexivity, belief-driven credit cycles, and self-referential expectations [11–13]. While these models reflect key aspects of reflexivity, they are either stochastic or equilibrium-based and do not feature deterministic chaos, Lyapunov instability, or strange attractors.

Prior studies discuss reflexivity largely in empirical or agent-based settings; here, we present a compact deterministic ODE formulation with an explicit sentiment state and verify low-dimensional chaos [10,12]. This formulation allows us to investigate how sentiment-driven feedback loops can generate and sustain chaos in macroeconomic dynamics.

Section 2 develops the model: formulation, behavioural assumptions, and well-posedness/dissipativity analysis. Section 3 presents the results: chaos diagnostics (largest Lyapunov exponent, spectra, and embeddings), equilibrium stability, state trajectories, phase portraits, and bifurcation scans. Section 4 discusses implications for reflexivity-driven instability and interpretation within behavioural macro-finance. Section 5 concludes with policy and control takeaways and directions for future work.

2. Materials and Methods

2.1. Model Formulation

Motivated by Soros's concept of a self-reinforcing feedback loop in market sentiment [10], we propose an integer-order extension of the Xin–Zhang system that incorporates a reflexive self-feedback term $m_4 w$ in the w-equation. This captures the behavioural insight that confidence is not only influenced by economic variables but also self-reinforces via feedback from market sentiment itself. The addition of this term enables the system to sustain higher levels of volatility and richer chaotic dynamics. Our proposed extended model becomes

$$\begin{aligned} \dot{x} &= z + (y - a)x + m_1 w, \\ \dot{y} &= 1 - by - x^2 + m_2 w, \\ \dot{z} &= -x - cz + m_3 w, \\ \dot{w} &= -xyz + m_4 w\,. \end{aligned} \tag{2}$$

The model couples interest x, investment y, prices z, and reflexive confidence w. High x imposes a quadratic halt on y; z cools when x is high and lifts with w; and w self-reinforces but is suppressed when x, y, z are jointly large. These feedbacks generate oscillatory, bursty motion.

- Interest rate x. Responds to inflation pressure z and to whether investment y exceeds a savings threshold a; larger $y - a$ tends to raise x.
- Investment demand y. Increases with confidence w but is suppressed by tighter rates via the term $-x^2$.
- Price index z. Decreases when x is high and can rise with w through spending pressure.
- Market confidence w. Reflexive through $m_4 w$; large simultaneous x, y, z activate the brake $-xyz$.

Table 1 presents suggested ranges for the model parameters based on established economic reasoning and prior studies on chaotic financial systems [7,10,14]. These values are selected to reflect realistic financial behaviours such as savings thresholds, investment sensitivity, price adjustment inertia, and the nonlinear influence of market confidence on system dynamics.

Table 1. Suggested parameter ranges based on economic intuition.

Parameter	Likely Range	Real-World Interpretation
a	0.5 to 2.5	Baseline savings threshold; higher a reflects more conservative economies
b	0.01 to 1	Cost per unit of investment; higher b implies more friction (e.g., taxes or capital costs)
c	0.5 to 3	Price index adjustment rate; high c indicates sticky prices or delayed inflation response
m_1	-0.5 to 10	Influence of market confidence on interest rate; positive m_1 links optimism to rising rates
m_2	0.1 to 10	Effect of confidence on investment demand; higher m_2 drives investment booms
m_3	-0.3 to 10	Impact of confidence on price index; positive m_3 may drive inflation
m_4	-0.3 to 3	Reflexivity coefficient; positive m_4 leads to self-reinforcing optimism or panic

2.2. Model Assumptions

The structure of the proposed model is based on several behavioural macroeconomic assumptions that describe how market confidence interacts with key financial variables:

- Interest rate and confidence: Market confidence tends to rise with accommodative monetary conditions, while tighter rates depress sentiment [15,16].
- Investment demand and confidence: Confidence and investment reinforce each other—optimism boosts investment plans; low confidence/uncertainty curbs them [17,18].
- Price index and confidence: Higher inflation erodes confidence and perceived purchasing power; strong sentiment can add demand pressure to prices [19,20].

- Nonlinear suppression effect: Following the Xin–Zhang system, confidence growth is damped when interest, investment, and prices are simultaneously high; we retain the multiplicative brake $(-xyz)$ [14].
- Reflexive feedback (novel): Confidence is self-reinforcing—improved outcomes bolster optimism—consistent with reflexivity and financial-instability views [10,21].

These assumptions collectively capture the dynamic interdependencies among economic variables and allow the model to reflect both stabilising and destabilising forces within a financial system.

The choice of parameter range for m_4 is guided by the dynamics of the w-equation:

$$\dot{w} = -xyz + m_4 w.$$

The term $-xyz$ acts as a nonlinear damping effect when x, y, and z are positive, while $m_4 w$ provides linear self-reinforcing growth of market confidence. For small m_4, damping can offset growth, keeping w bounded. If m_4 is sufficiently large, the growth term dominates over most of the trajectory, and the equation reduces to $\dot{w} \approx m_4 w$, yielding exponential divergence. Because w also appears in the x-, y-, and z-equations, such growth destabilises the entire system. This mechanism imposes a practical upper limit on m_4 for bounded chaotic behaviour, and we restrict simulations to values below this threshold.

2.3. Well-Posedness and Positivity Analysis

2.3.1. Well-Posedness

We consider the extended financial system defined by (2) where $x(t), y(t), z(t), w(t) \in \mathbb{R}$ and the parameters $a, b, c, m_1, m_2, m_3, m_4$ are real constants with $a, b, c \geq 0$.

Each right-hand side is a continuously differentiable function of (x, y, z, w), and thus locally Lipschitz in $\mathbb{R}^4$. By the Picard–Lindelöf theorem, the system admits a unique local solution for any initial condition in $\mathbb{R}^4$. Hence, the system is locally well-posed.

To investigate global existence, we define the Lyapunov function:

$$V(x, y, z, w) = \frac{1}{2}(x^2 + y^2 + z^2 + w^2).$$

Note that this function satisfies the standard properties:

- Positive definite: $V(x, y, z, w) > 0$ for all $(x, y, z, w) \neq 0$.
- Radially unbounded: $V \to \infty$ as $\|(x, y, z, w)\| \to \infty$.

The time derivative of V along system trajectories is

$$\dot{V} = x\dot{x} + y\dot{y} + z\dot{z} + w\dot{w},$$

which expands to the polynomial in x, y, z, w:

$$\dot{V} = -ax^2 - by^2 - cz^2 + y + m_1 xw + m_2 yw + m_3 zw + m_4 w^2 - xyzw.$$

Observe that the leading quadratic terms $-ax^2$, $-by^2$, and $-cz^2$ contribute negatively to $\dot{V}$ and thus act as stabilising components in the system.

To control the growth of positive mixed terms $m_1 xw$, $m_2 yw$, and $m_3 zw$, we can apply Young's inequality:

$$ab \leq \frac{\epsilon a^2}{2} + \frac{b^2}{2\epsilon}, \quad \text{for any } \epsilon > 0.$$

For example, the term m_1xw satisfies

$$m_1xw \leq \frac{\epsilon x^2}{2} + \frac{m_1^2 w^2}{2\epsilon}.$$

Applying Young's inequality to the bilinear terms and noting that the trajectories we study remain in the non-negative orthant, so that $-xyzw \leq 0$, we obtain the bound

$$\dot{V} \leq -ax^2 - by^2 - cz^2 + y + \frac{\epsilon_1}{2}x^2 + \frac{m_1^2}{2\epsilon_1}w^2 + \frac{\epsilon_2}{2}y^2 + \frac{m_2^2}{2\epsilon_2}w^2 + \frac{\epsilon_3}{2}z^2 + \frac{m_3^2}{2\epsilon_3}w^2 + m_4w^2.$$

Hence,

$$\dot{V} \leq C_1 - C_2(x^2 + y^2 + z^2) + C_3w^2,$$

$$C_1 = \frac{1}{2\delta}, \quad \text{(from bounding } y \text{ using } y \leq \frac{1}{2\delta} + \frac{\delta y^2}{2}),$$

$$C_2 = \min\left(a - \frac{\epsilon_1}{2},\ b - \frac{\delta}{2} - \frac{\epsilon_2}{2},\ c - \frac{\epsilon_3}{2}\right),$$

$$C_3 = \frac{m_1^2}{2\epsilon_1} + \frac{m_2^2}{2\epsilon_2} + \frac{m_3^2}{2\epsilon_3} + m_4.$$

Here, $\epsilon_1, \epsilon_2, \epsilon_3, \delta > 0$ are small constants chosen to balance the mixed terms using Young's inequality.

Choosing $\epsilon_i > 0$ sufficiently small ensures that the negative quadratic terms dominate; hence $\dot{V} \leq C - \alpha V$ for some constants $C \geq 0$ and $\alpha > 0$. This implies the trajectories are ultimately bounded, confirming the system is dissipative. When the parameters m_i, particularly m_4, are sufficiently small, the system exhibits dissipativity, and $V(t)$ remains bounded for all t. This implies that all trajectories are ultimately bounded and the system is globally well-posed in this parameter regime.

2.3.2. Positivity

For economic interpretation, it is desirable that x, y, z, w (interest rate, investment demand, price index, market confidence) remain non-negative. The system, however, does not guarantee positivity preservation for all parameter choices: on the boundaries $x = 0$ and $w = 0$, the vector field is inward ($\dot{x} \geq 0$, $\dot{w} = 0$), whereas at $y = 0$ or $z = 0$, the signs of $\dot{y}$ and $\dot{z}$ depend on x, w and parameters m_2, m_3. Hence the non-negative orthant $\mathbb{R}^4_{\geq 0}$ is not invariant in general. In our simulations, we restrict parameters and initial conditions so that all state variables remain non-negative over the reported horizons; we do not claim global positivity invariance.

2.3.3. Diagnostics Used

Chaotic dynamics. We use "chaotic" to denote trajectories with sensitive dependence on initial conditions. Operationally, chaos is evidenced by a positive largest Lyapunov exponent $L_1 > 0$, so that small perturbations grow on average as

$$\|\delta x(t)\| \approx \|\delta x(0)\|\, e^{L_1 t}.$$

(Classical topological criteria involve mixing and dense periodic orbits; for numerical studies, $L_1 > 0$ is the standard indicator; see, e.g., [22,23].)

Lyapunov exponents. For the smooth autonomous system $\dot{x} = f(x)$ with flow ϕ^t, the Lyapunov spectrum $\{L_i\}_{i=1}^n$ quantifies mean exponential growth/decay rates of infinitesimal perturbations along an orbit (Oseledets theorem). The largest exponent is

$$L_1 = \lim_{t\to\infty} \frac{1}{t} \log \frac{\|\mathrm{D}\phi^t(x_0)v\|}{\|v\|}, \qquad v \neq 0.$$

For autonomous flows, one exponent is typically 0 (time-shift symmetry). A negative sum $\sum_{i=1}^{n} L_i < 0$ indicates average phase-volume contraction (dissipativity).

Kaplan–Yorke (Lyapunov) dimension. Let $S_j = \sum_{i=1}^{j} L_i$ and choose j as the largest index with $S_j \geq 0$. The Kaplan–Yorke (Lyapunov) dimension [24] is

$$D_{\mathrm{L}} = j + \frac{S_j}{|L_{j+1}|},$$

which estimates the effective (fractal) dimension of the attractor.

Delay-embedding. Given a scalar observable $y(t_k)$, we reconstruct the state via delay vectors

$$Y_k = \big(y(t_k),\, y(t_k - \tau),\, \ldots,\, y(t_k - (m-1)\tau)\big) \in \mathbb{R}^m.$$

Under generic conditions, choosing a sufficiently large m yields an embedding of the underlying dynamics (Takens' theorem [25]). In practice, we select the delay τ at the first minimum of the average mutual information (or near the first zero of the autocorrelation), and the embedding dimension m by the false nearest neighbors criterion [23]. The chosen (τ, m) values are reported alongside our reconstructions.

3. Results

In this section, we adopt the baseline parameter values from the Xin–Zhang system (1) as follows:

$$a = 2.1, \quad b = 0.01, \quad c = 2.6, \quad m_1 = 8.4, \quad m_2 = 6.4, \quad m_3 = 2.2, \quad m_4 = 0.001, \quad (3)$$

where m_4 is the additional parameter introduced in our extended model to capture the self-reinforcing feedback loop in market confidence.

For dynamic simulations, we restricted the sweep of m_4 to the interval $[0, 0.005]$ (see Section 2.2) to avoid finite-time blow-up and to ensure well-posedness (see Section 2.3.1). Unless stated otherwise, we restrict parameter scans to empirically feasible ranges identified from the peak–scan diagnostics reported in Appendix A (Table A1; see also Figures A1 and A2). Fixed initial conditions are $x(0) = 1$, $y(0) = 5$, $z(0) = 4$, and $w(0) = 3$.

All simulations were performed in MATLAB R2019a using `ode45` with `RelTol` $= 10^{-8}$ and `AbsTol` $= 10^{-10}$. Unless otherwise stated, the output time step was $\Delta t = 0.01$, the time horizon was $T = 500$, and the transient discard was 80%. The Benettin–Wolf algorithm [26] was used to compute Lyapunov spectra, with re-orthonormalization interval $\tau = 1$ and initial perturbation $\delta_0 = 10^{-8}$.

3.1. Chaotic Diagnostics at the Baseline Parameter Set

To verify chaos under the baseline parameters, we combined four complementary tests: the largest Lyapunov exponent (LLE), a frequency-domain check, a Poincaré section, and a nearby-trajectory divergence test. The finite-time LLE converges to a small but positive value, $\lambda_1 \approx 9.65 \times 10^{-3}\,\mathrm{time}^{-1}$ (Figure 1); this implies an e-folding time $T_e \approx 1.04 \times 10^2$ and a doubling time $T_2 \approx 72$ time units, indicating *weak* but sustained sensitive dependence. The post-transient power spectrum is broadband rather than a few sharp lines (Figure 2), inconsistent with purely periodic or quasi-periodic motion. Poincaré sections form dispersed, multi-strip sets instead of closed curves (Figure 3), and the distance between two trajectories beginning $\mathcal{O}(10^{-6})$ apart grows irregularly before saturating on the attractor

(Figure 4). These diagnostics consistently support a strange attractor with slow exponential separation ("weak chaos") in this parameter regime.

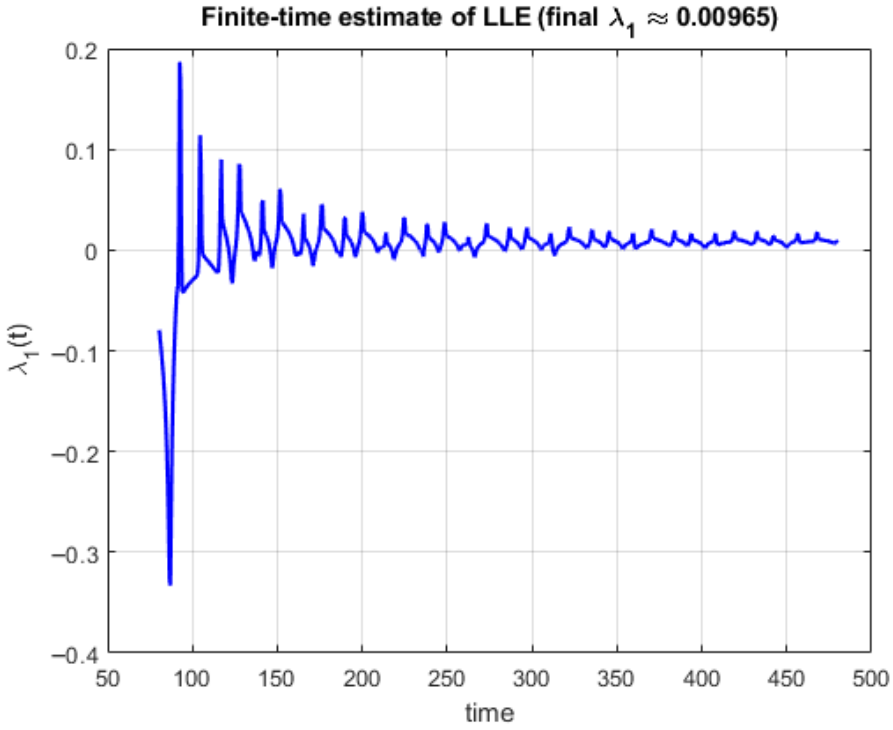

Figure 1. Finite-time largest Lyapunov exponent estimate $\lambda_1(t)$ converging to $\lambda_1 \approx 9.65 \times 10^{-3}$ time^{-1}.

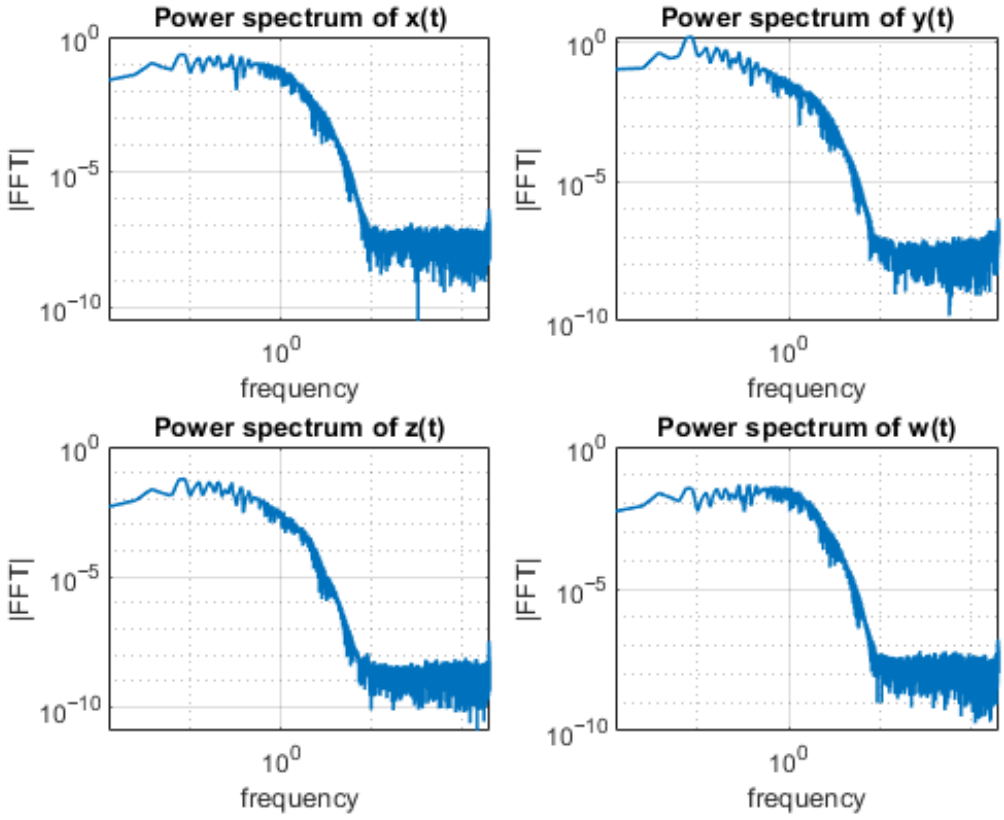

Figure 2. Power spectrum of $x(t), y(t), z(t), w(t)$ (post-transient) showing a broadband continuum characteristic of aperiodic/chaotic dynamics.

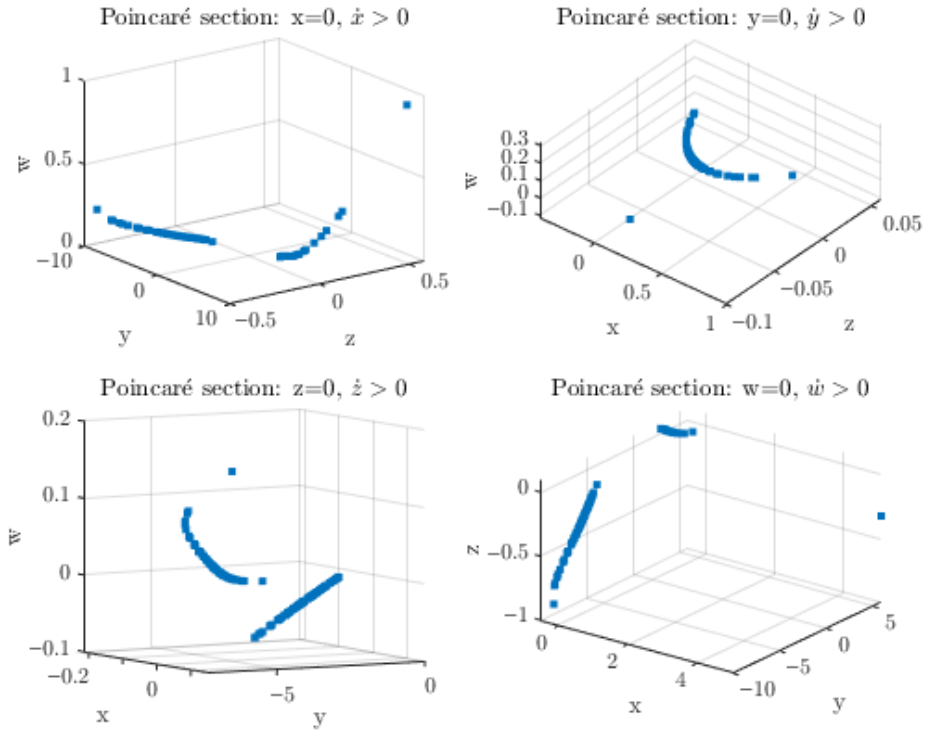

Figure 3. Poincaré sections. The scattered multistrip set is incompatible with a single periodic orbit.

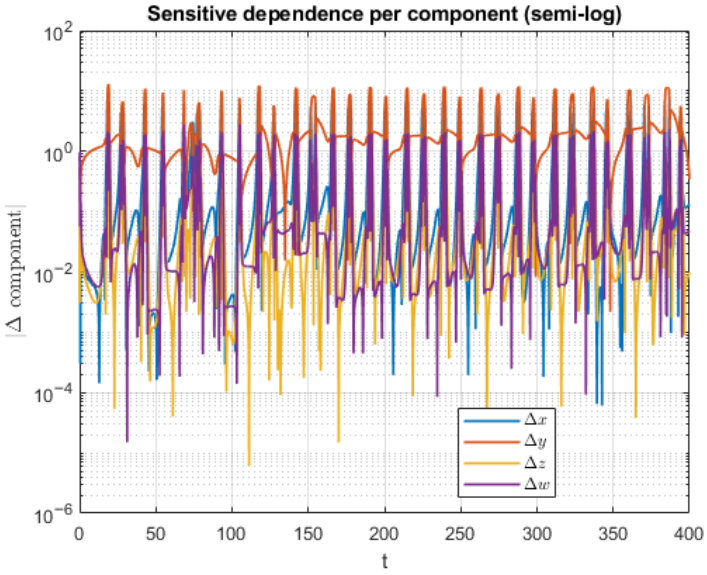

Figure 4. Sensitive dependence: growth and eventual saturation of the separations $\|\Delta x(t)\|_2$, $\|\Delta y(t)\|_2$, $\|\Delta z(t)\|_2$, and $\|\Delta w(t)\|_2$ between two trajectories started 10^{-6} apart.

3.2. Lyapunov Exponent Spectrum Analysis

To examine the dynamical behaviour, we compute the full Lyapunov spectrum using the Benettin orthonormalization scheme and the Wolf et al. algorithm [26–28].

Figures 5 and 6 present the Lyapunov exponents as the feedback parameters m_1, m_2, m_3, m_4, and the original system parameters a, b, c are varied. Across all parameter scans, we observed, at most, one positive Lyapunov exponent; whenever chaos appears, the spectrum takes the canonical autonomous-flow form $L_1 > 0$, $L_2 \approx 0$, $L_3, L_4 < 0$, with L_1 modest but nonzero, i.e., one expanding, one neutral, and two contracting directions—indicating chaos.

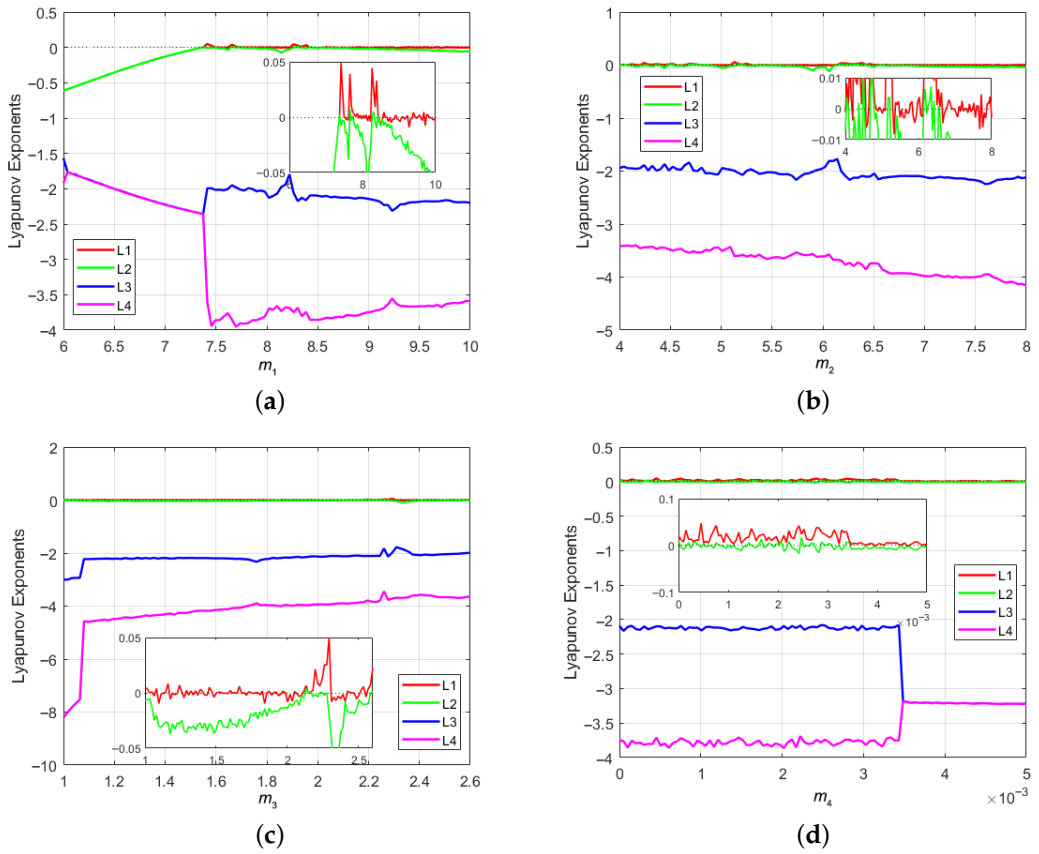

Figure 5. Lyapunov exponents of the system for varying m values: (**a**) m_1; (**b**) m_2; (**c**) m_3; and (**d**) m_4.

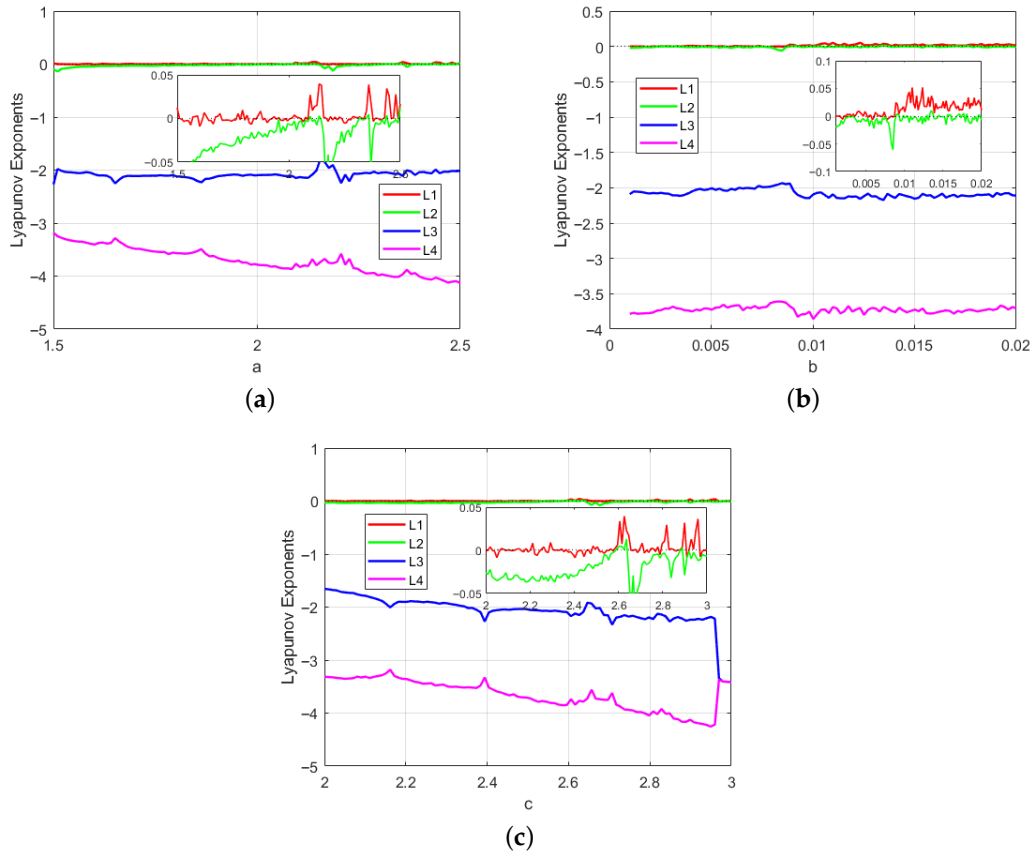

Figure 6. Lyapunov exponents of the system for varying (**a**) a, (**b**) b, and (**c**) c values.

3.2.1. Lyapunov Dimension and Dynamical Transitions

We use the Kaplan–Yorke dimension for attractor complexity [24].

Figures 7 and 8 show broad plateaus near $D_L \approx 0, 1, 2$ separated by narrow transition bands revealing alternating intervals of low-dimensional dynamics and higher-dimensional attractors.

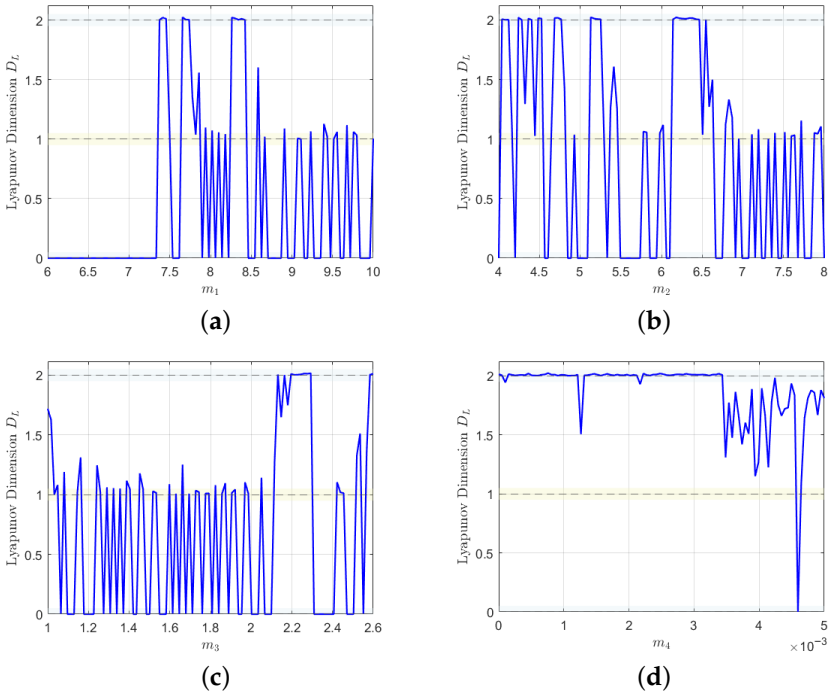

Figure 7. Variation in the Lyapunov (Kaplan–Yorke) dimension D_L as a function of feedback parameters: (**a**) m_1, (**b**) m_2, (**c**) m_3, and (**d**) m_4. The plots reveal alternating intervals of low-dimensional dynamics and higher-dimensional attractors.

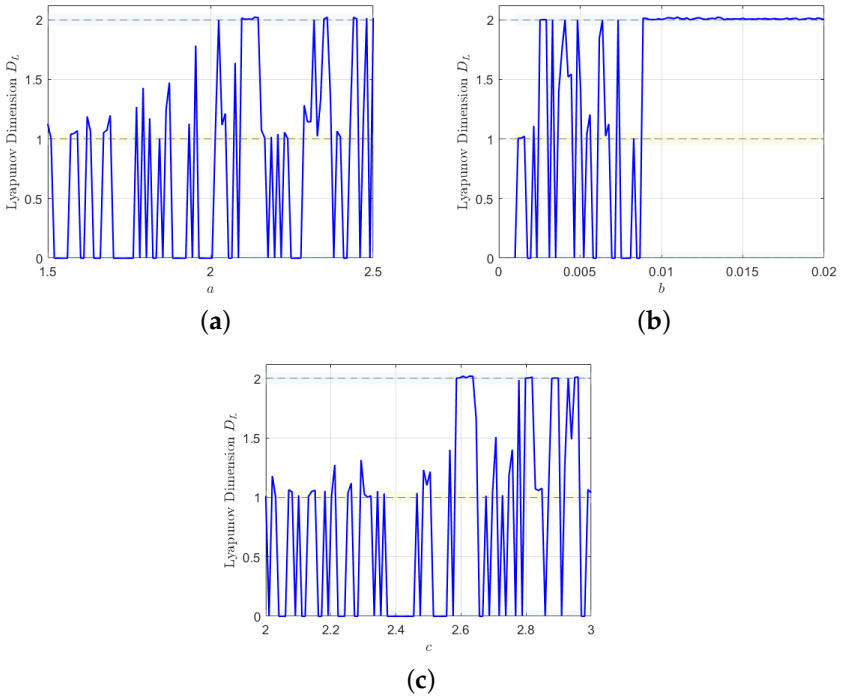

Figure 8. Variation in the Lyapunov (Kaplan–Yorke) dimension D_L as a function of structural parameters: (**a**) a, (**b**) b, and (**c**) c.

Figure 9 illustrates the variation in the Lyapunov spectrum (L_1, L_2, L_3, L_4) with respect to changes in each initial condition while keeping the other three fixed. In all cases, the largest exponent L_1 remains strictly positive, confirming the persistence of chaotic dynamics throughout the tested ranges of initial conditions. The second exponent L_2 remains close to zero, as expected for autonomous systems due to the neutral direction associated with the flow. The remaining exponents L_3 and L_4 are negative, indicating contraction along stable directions. The insets highlight the near-zero range, revealing small fluctuations in L_1 that suggest moderate sensitivity to perturbations in the initial state but no abrupt transitions in the underlying attractor. These results demonstrate that the system's chaotic behaviour is robust to moderate variations in the starting conditions.

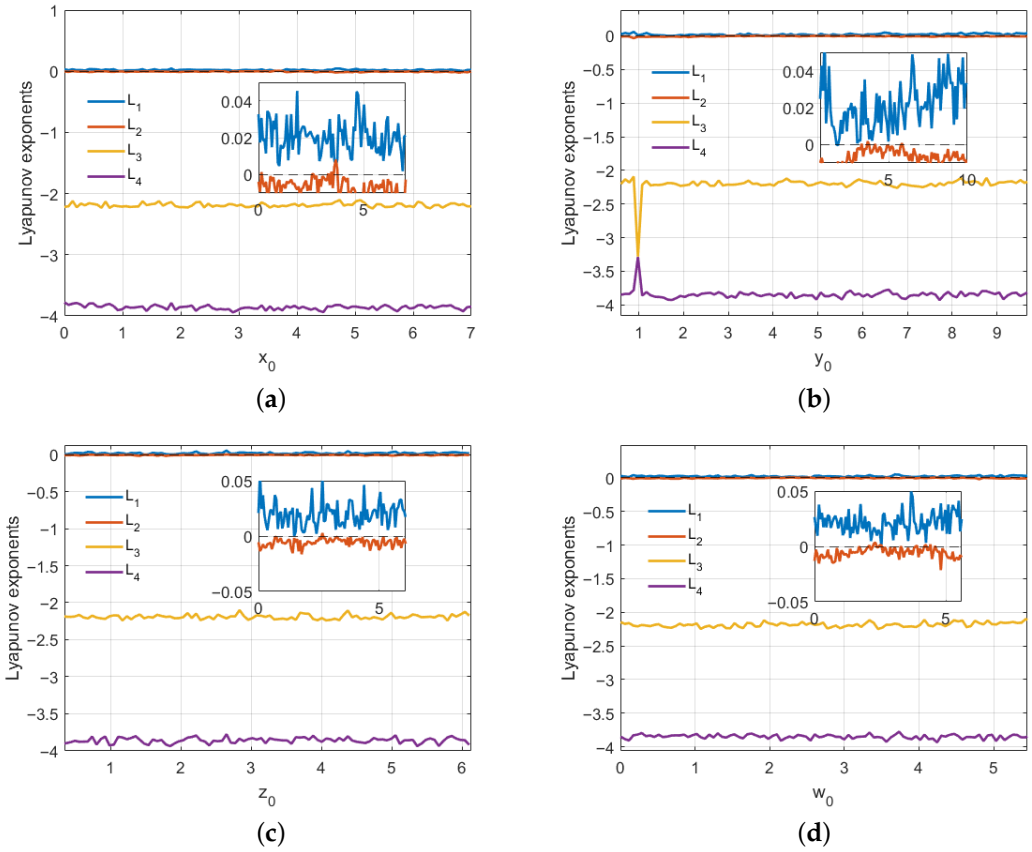

Figure 9. Variation in the Lyapunov spectrum (L_1, L_2, L_3, L_4) of the extended financial system with respect to (**a**) x_0, (**b**) y_0, (**c**) z_0, and (**d**) w_0 while keeping the other three initial conditions fixed.

3.2.2. Dissipativity and Entropy

For smooth autonomous flows, the sum of Lyapunov exponents equals the long-time mean phase–space divergence along typical trajectories, $\sum_{i=1}^{4} L_i \approx \langle \nabla \cdot f(x(t)) \rangle_t$. At our baseline, we obtain $\sum_i L_i \approx -5.90$ and $\langle \nabla \cdot f \rangle_t \approx -5.77$ (see the divergence trace in Figure 10), which agree within $\approx 2.3\%$ and are both negative, confirming dissipativity. Moreover, the Kolmogorov–Sinai entropy satisfies $h_{KS} = \sum_{L_i > 0} L_i$; here, $h_{KS} \approx 1.76 \times 10^{-2} > 0$, indicating positive information production and thus chaotic dynamics.

3.2.3. Delay-Embedding

Using average mutual information, the first minimum occurs at $\tau^\star \approx 1.05$ (Figure 11a, left); the ACF crosses zero at a comparable lag (Figure 11a, right). The false-nearest-neighbours curve falls steeply and is $\leq 10\%$ by $m = 3$ (Figure 11b), so we adopt $(\tau^\star, m) = (1.05, 3)$. The 2D/3D reconstructions (Figure 11c,d) show a thin, folded manifold with stretching rather than a single closed curve, consistent with a low-dimensional deterministic

attractor. Together with the positive largest Lyapunov exponent reported, these embeddings support the presence of chaotic dynamics.

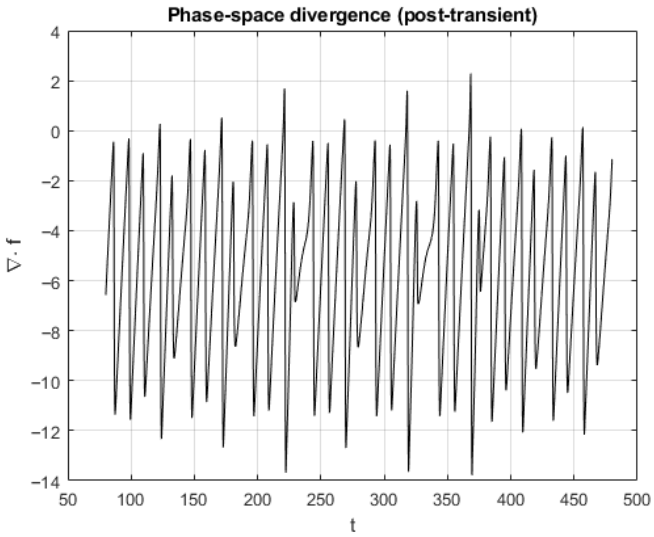

Figure 10. Running time average of the phase–space divergence $\nabla \cdot f(x(t))$ along the same trajectory. The long-time mean is $\langle \nabla \cdot f \rangle_t \approx -5.77$. $\sum_i L_i = -5.90$ and, together with $h_{\mathrm{KS}} = \sum_{L_i>0} L_i \approx 1.76 \times 10^{-2}$, confirms dissipativity and positive entropy production.

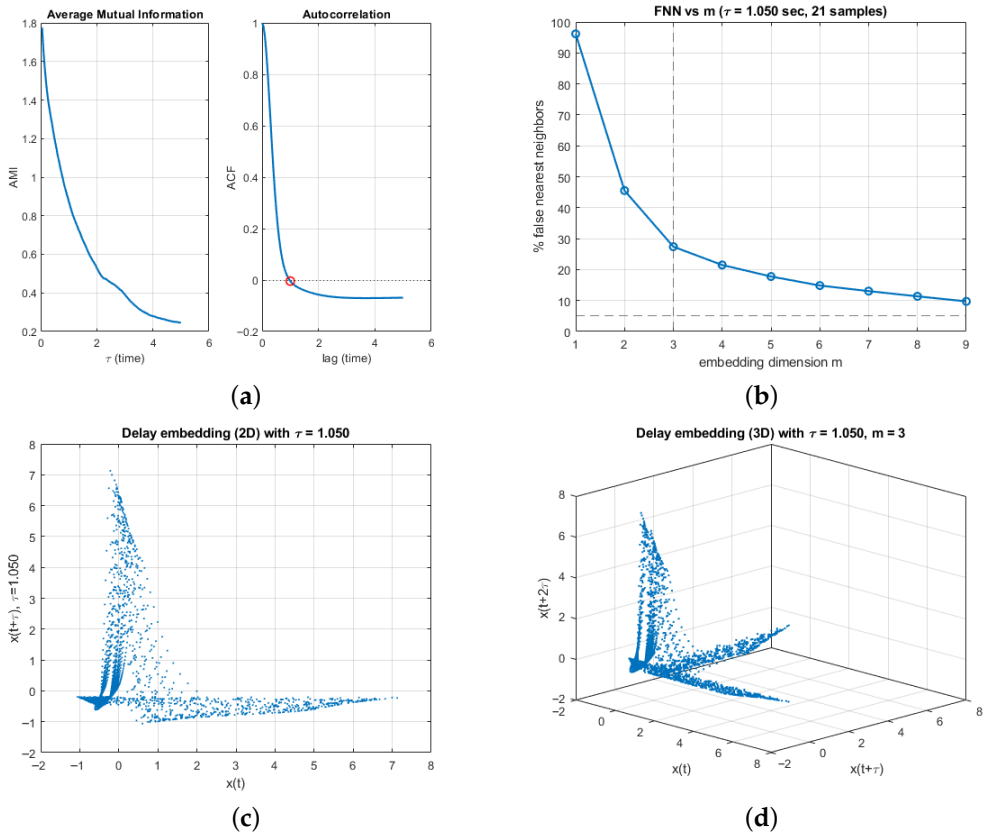

Figure 11. Delay-embedding diagnostics and reconstructions for $x(t)$ with optimal delay $\tau^\star = 1.050$ and embedding dimension $m = 3$: (**a**) Average mutual information (**left**) and autocorrelation (**right**) vs. lag; the first AMI minimum occurs at $\tau^\star$ and the ACF crosses zero at a comparable lag. (**b**) False nearest neighbors (%) versus embedding dimension m; the rate drops below 10% by $m = 3$. (**c**) 2D delay embedding $(x(t),\, x(t - \tau^\star))$. (**d**) 3D delay embedding $(x(t),\, x(t - \tau^\star),\, x(t - 2\tau^\star))$.

3.3. Equilibrium and Stability Analysis

Because closed-form equilibria are not available when the confidence state is active ($w \neq 0$), we use numerical continuation. For each parameter $p \in \{m_1, m_2, m_3, m_4, a, b, c\}$, we sweep a grid of values and solve the steady-state system as follows:

$$\dot{x} = \dot{y} = \dot{z} = \dot{w} = 0$$

with `fsolve` (seeding each step with the previous solution), and then evaluate the Jacobian J at the equilibrium $E^* = (x^*, y^*, z^*, w^*)$. Local stability is assessed from the spectrum $\{\lambda_i\}_{i=1}^4$ of J.

Figures 12 and 13 show smooth changes in the equilibrium components across all sweeps, consistent with continuous parameter dependence. The stability panels reveal that, over the scanned ranges, at least one eigenvalue real part remains positive for essentially all settings, so the equilibrium is *not* locally asymptotically stable.

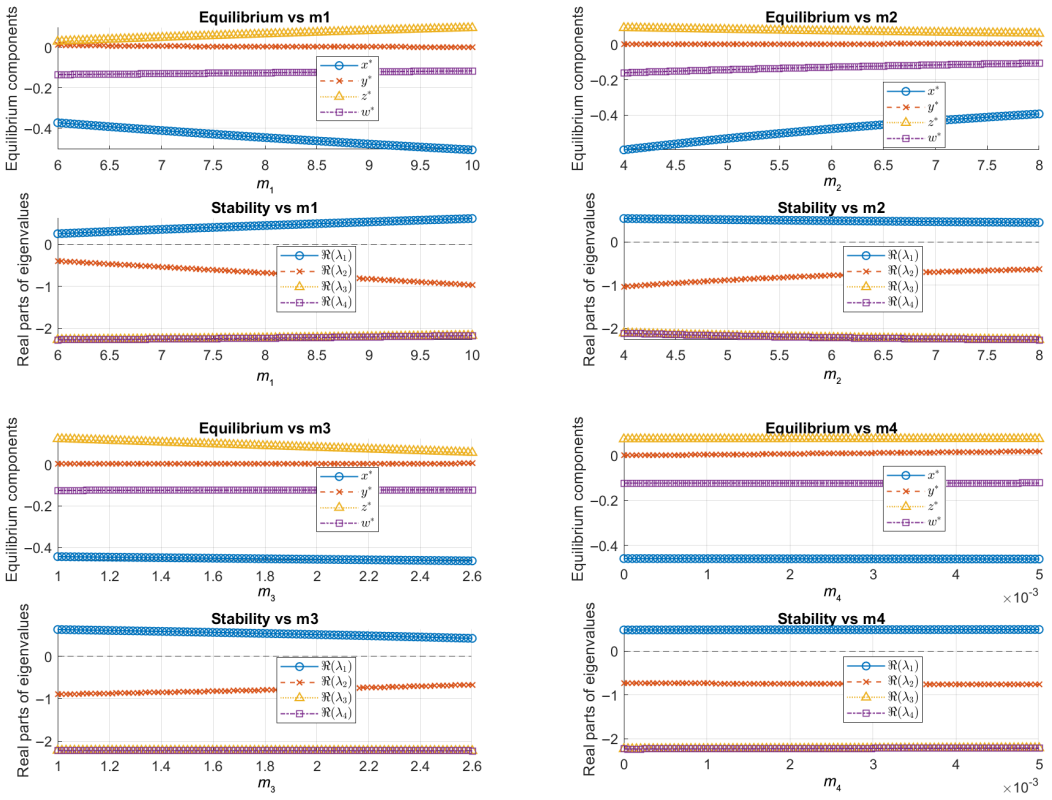

Figure 12. Equilibrium and stability versus the feedback parameters m_1, m_2, m_3, m_4. (**Top**): equilibrium components (x^*, y^*, z^*, w^*). (**Bottom**): real parts of the Jacobian eigenvalues at equilibrium. Persistent $\max_i \Re(\lambda_i) > 0$ indicates an unstable equilibrium.

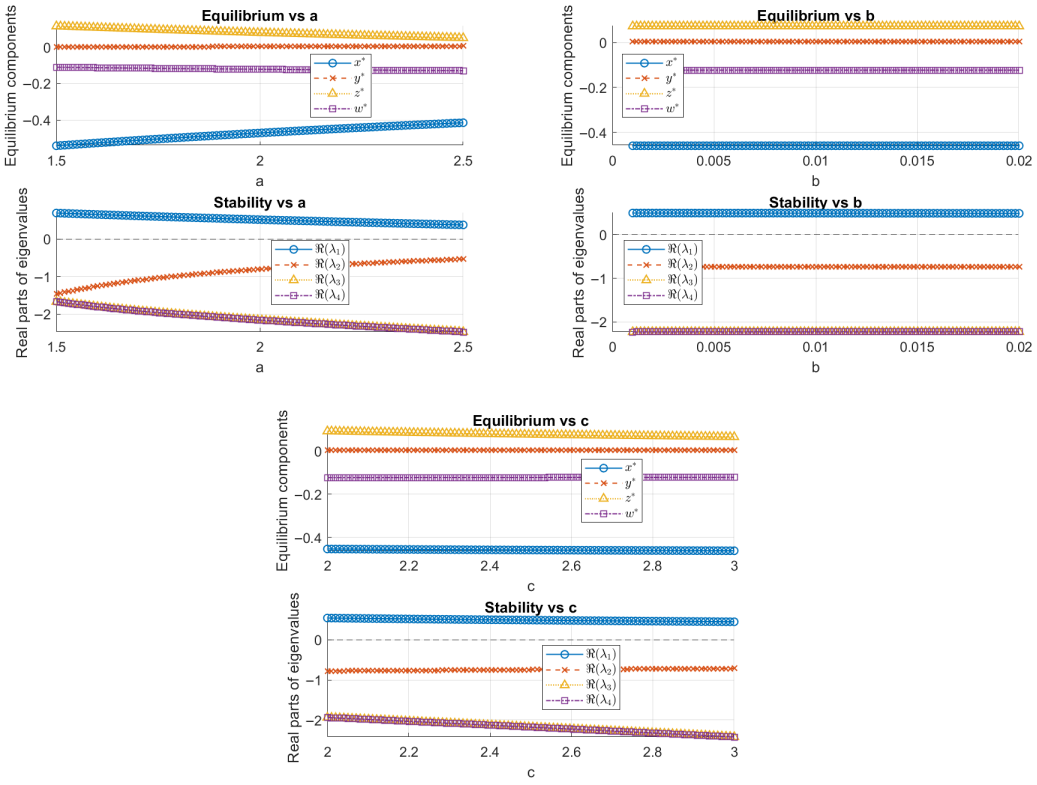

Figure 13. Equilibrium and stability versus the structural parameters a, b, c. (**Top**): equilibrium components. (**Bottom**): real parts of eigenvalues.

Consistent with the global diagnostics reported earlier, intervals where $\Re(\lambda_{\max}) > 0$ align with elevated Lyapunov complexity, supporting the interpretation that reflexive feedback maintains oscillatory/chaotic motion rather than convergence to a fixed point.

To illustrate these findings with a representative example, we examine the equilibrium structure at the baseline parameter values given in (3). At these settings, the system admits a non-trivial equilibrium point:

$$E_B = (x^*, y^*, z^*, w^*) \approx (2.1792,\ -0.00078,\ -0.3425,\ 0.5858).$$

The Jacobian evaluated at E_B reveals a pair of complex conjugate eigenvalues with positive real parts, indicating an unstable spiral–saddle configuration. This local instability is consistent with the global behaviour observed in the numerical simulations and bifurcation diagrams. Figure 14 presents the corresponding phase portraits, which display high-dimensional chaotic trajectories, further highlighting the active role of market confidence in driving instability.

When $w = 0$, the extended model reduces to the original three-dimensional chaotic financial system introduced by [7]. The bifurcation structure and stability of equilibria in that reduced model were thoroughly investigated in their work, including conditions for saddle-node and Hopf bifurcations. Their classification of strange attractors in the three-dimensional system supports the interpretation that chaos is already embedded in the core dynamics and is further enriched by introducing dynamic market confidence as a fourth state variable.

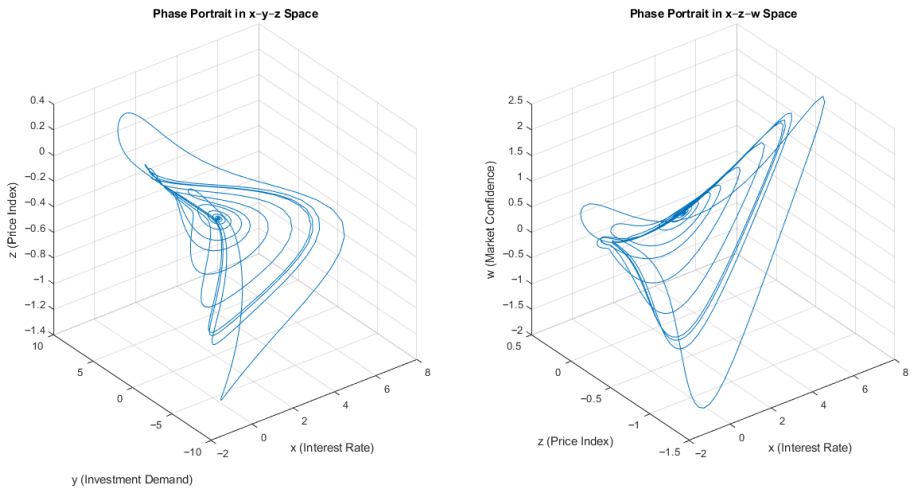

Figure 14. Phase portraits of the extended financial system projected into (**left**) x–y–z space and (**right**) x–z–w space. The projections show complex, aperiodic motion, with market confidence acting as an active driver in system instability.

3.4. State Trajectories, Bifurcation Diagrams, and Phase Portraits

3.4.1. State Trajectories

Using the original parameter settings (3) and initial conditions, we simulated the system (2) over a time span of $T = 500$ with a step size of $\Delta t = 0.01$, and plotted the state trajectories of all four variables to observe the emergence of chaotic behaviour.

The state trajectories generated from the initial condition $(x_0, y_0, z_0, w_0) = (1,\ 5,\ 4,\ 3)$ with $m_4 = 0.001$ exhibit irregular, aperiodic behaviour, providing clear evidence of chaos in the system.

Figure 15 shows the state trajectories at baseline: $x(t)$ and $w(t)$ display bursting, $y(t)$ has a sawtooth pattern with slow ramps and sharp drops, and $z(t)$ oscillates irregularly with small amplitude around zero. These trajectories indicate chaos; even small confidence feedback m_4 generates complex, unpredictable motion.

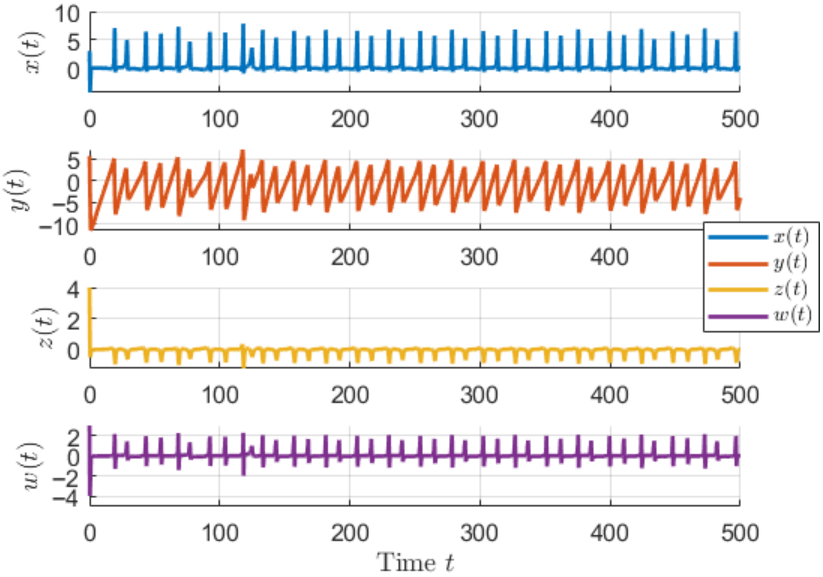

Figure 15. State trajectories of the state variables $x(t)$, $y(t)$, $z(t)$, and $w(t)$ simulated from the initial condition $(x_0, y_0, z_0, w_0) = (1, 5, 4, 3)$ with fixed parameter values from Equation (3). The irregular and non-repeating trajectories indicate chaotic behaviour in the system.

To assess the sensitivity of the system to initial conditions, we performed perturbation experiments in which small deviations were introduced to individual components of the nominal initial state $\mathbf{X}_0 = [1, 5, 4, 3]$. Three perturbed cases were considered: IC2 with $x_0 = 1.05$, IC3 with $y_0 = 4.95$, and IC4 with $z_0 = 4.05$, while keeping the other components fixed at their nominal values. Figure 16 shows the resulting state trajectories for all four state variables over a simulation horizon of $t \in [0, 500]$.

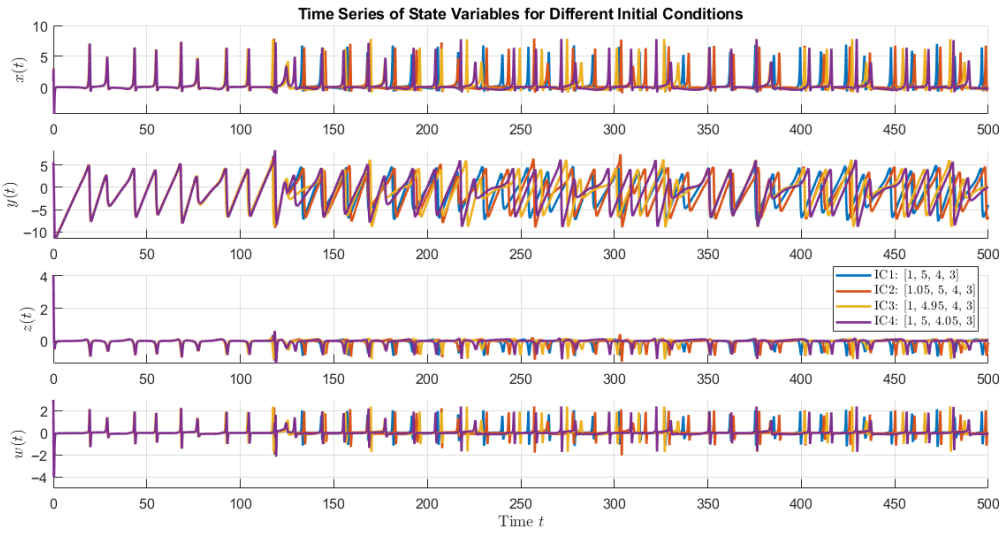

Figure 16. State trajectories of all four state variables $x(t)$, $y(t)$, $z(t)$, and $w(t)$ under small perturbations to the initial conditions. The nominal initial condition is $\mathbf{X}_0 = [1, 5, 4, 3]$. Perturbations of magnitude 0.05 were applied to one component at a time, producing IC2: $x_0 = 1.05$, IC3: $y_0 = 4.95$, and IC4: $z_0 = 4.05$, with all other components unchanged.

In each subplot, the initially close trajectories diverge markedly as time progresses, despite the perturbations being as small as 0.05. This rapid divergence indicates the presence of sensitive dependence on initial conditions, a hallmark of chaotic dynamics. Such behaviour implies that precise long-term prediction of the system's state is practically impossible, even when initial measurements are highly accurate.

3.4.2. Phase Portraits

Figure 17 shows projections of the four-dimensional attractor onto several three-dimensional subspaces. In standard 2D/3D projections, the trajectories lie on thin, folded manifolds that are densely visited—typical of strange attractors—consistent with a positive largest Lyapunov exponent and the Kaplan–Yorke dimension estimates. As a geometric check, we estimated the correlation (Grassberger–Procaccia) dimension from long trajectories, obtaining $D_2 \approx 1.43$ over the scaling window $r \in [12.2, 18]$ (log–log indices $[20, 27]$), in line with the Lyapunov- and Kaplan–Yorke-based evidence of low-dimensional chaos.

3.4.3. Bifurcation Analysis

Bifurcation diagrams were generated to examine how the system's long-term dynamics evolve as key parameters are varied individually while keeping all others fixed at their baseline values (3). For each parameter sweep, the system was integrated for a total time of $T_{\text{total}} = 1000$ using the `ode45` solver in MATLAB with $\Delta t = 0.01$, relative tolerance 10^{-6}, and absolute tolerance 10^{-8}. The first 80% of each trajectory was discarded to eliminate transients, and the remaining steady-state portion was processed to extract peaks with a minimum prominence of 10^{-3}, enabling clear identification of periodic and chaotic structures.

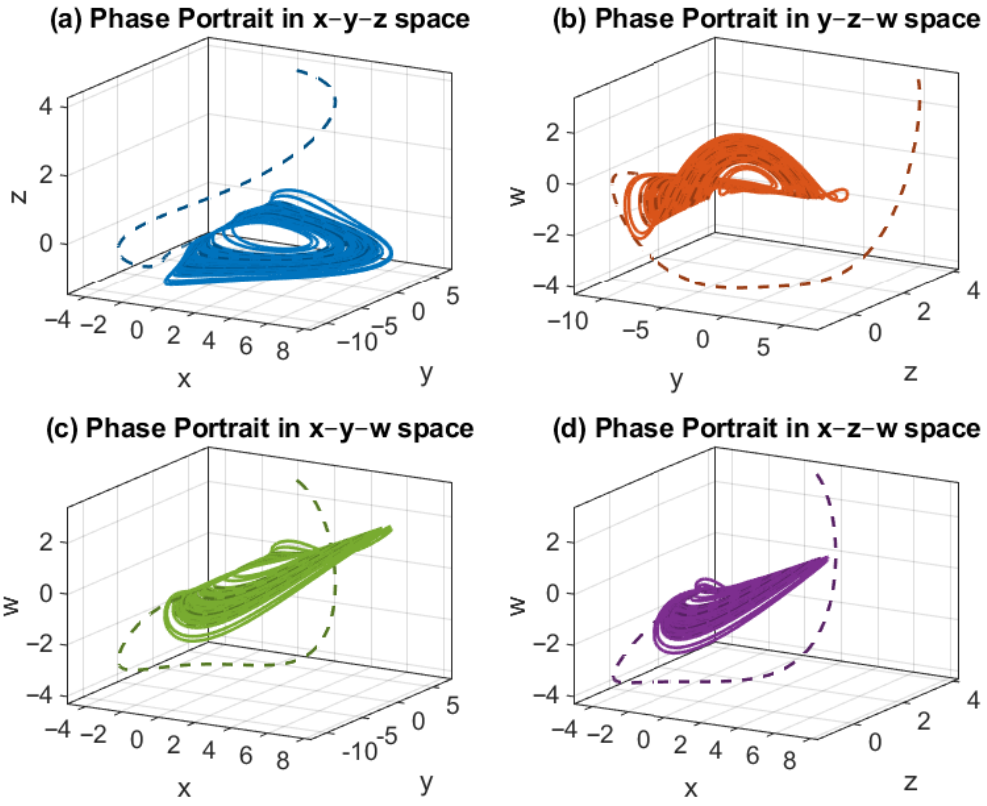

Figure 17. Phase portraits of the extended financial system projected onto different 3D subspaces. The trajectories exhibit complex, aperiodic motion with folding and stretching, confirming chaotic dynamics. Projections involving the market confidence variable w emphasise its active role in destabilising the system.

For $m_1 \in [4, 10]$ (see Figure 18), trajectories progress from stable fixed points through a period-doubling cascade into chaos, with intermittent periodic windows; irregularity is strongest in $x(t)$ and $y(t)$, while $z(t)$ remains lower in amplitude yet still fluctuates chaotically.

For $m_2 \in [0, 10]$ (Figure 19), chaos begins near $m_2 \approx 4.5$, persists in a broadband up to ≈ 6.2, then restabilises—indicating a feedback sensitivity threshold.

For $m_3 \in [0, 2.5]$ (Figure 20), dynamics are periodic at small values, followed by an abrupt onset of chaos near $m_3 \approx 2.1$.

For small positive m_4 (up to 0.005) (Figure 21), strong irregularity appears across all variables, confirming the destabilising effect of self-feedback.

Varying structural parameters shows similar routes: for $a \in [1.5, 2.5]$ (Figure 22), chaos dominates for $a \geq 2.1$ with occasional periodic windows; for $b \in [0, 0.02]$ (Figure 23), chaos emerges early and spans most of the range with only narrow periodic intervals; for $c \in [2, 3]$ (Figure 24), behaviour remains regular until about $c \approx 2.6$, beyond which chaos persists.

Overall, both confidence-related (m_1–m_4) and structural (a, b, c) parameters drive transitions from steady/periodic motion to chaos via period-doubling, punctuated by periodic windows, and the strength of chaotic signatures varies across state variables.

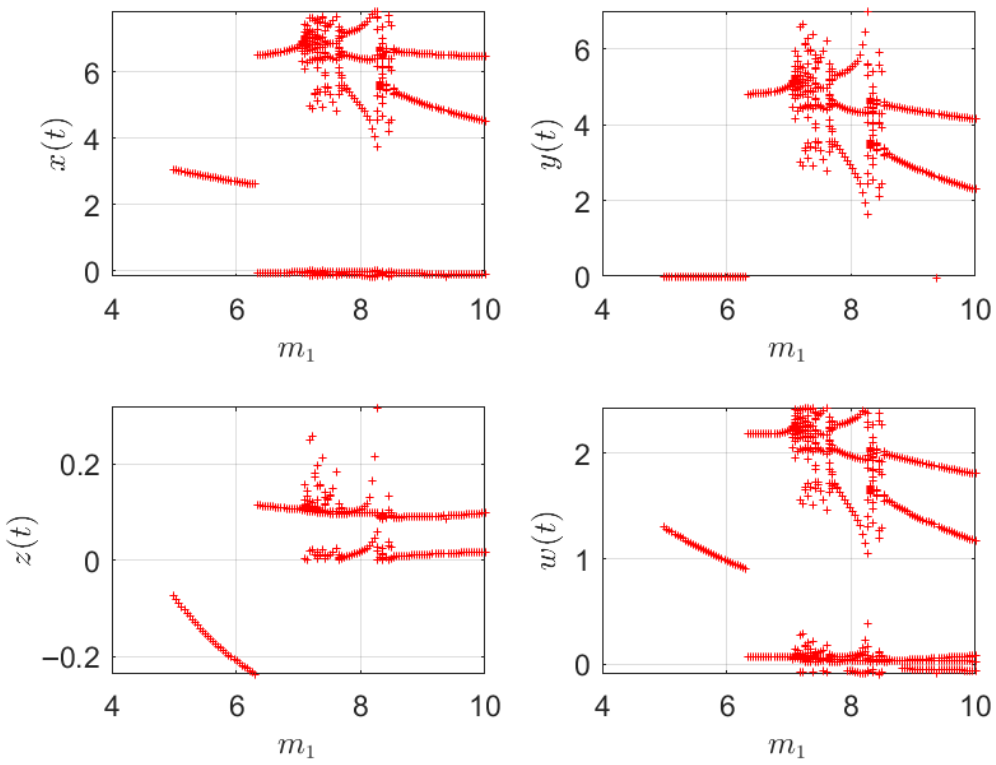

Figure 18. Bifurcation diagrams of $x(t)$, $y(t)$, $z(t)$, and $w(t)$ with respect to m_1. The system transitions from periodic motion to chaos via period-doubling, with intermittent periodic windows.

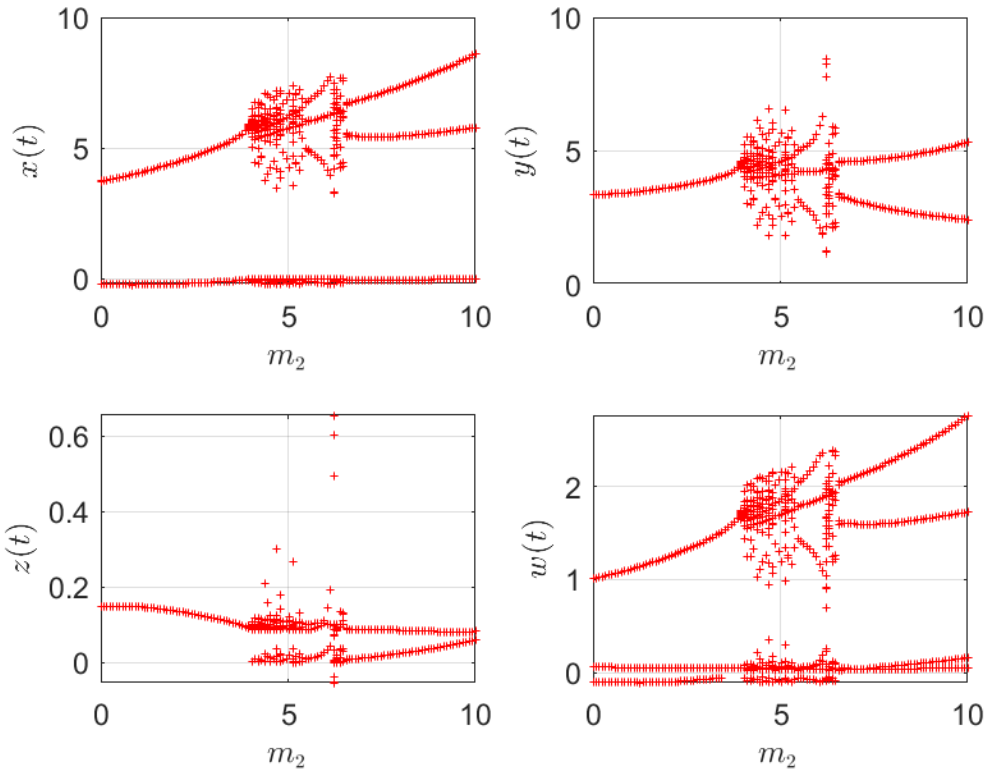

Figure 19. Bifurcation diagrams of $x(t)$, $y(t)$, $z(t)$, and $w(t)$ with respect to m_2. A pronounced chaotic band emerges around $m_2 \approx 4.5$ before the system restabilises.

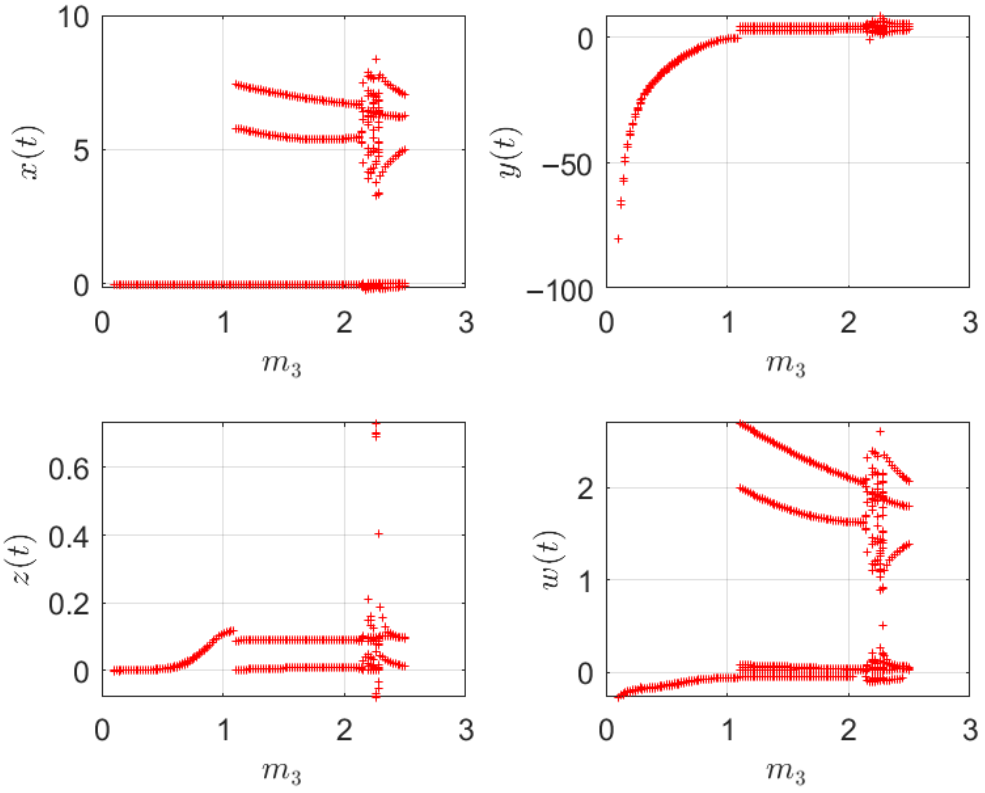

Figure 20. Bifurcation diagrams of $x(t)$, $y(t)$, $z(t)$, and $w(t)$ with respect to m_3. Chaos emerges abruptly near $m_3 \approx 2.1$.

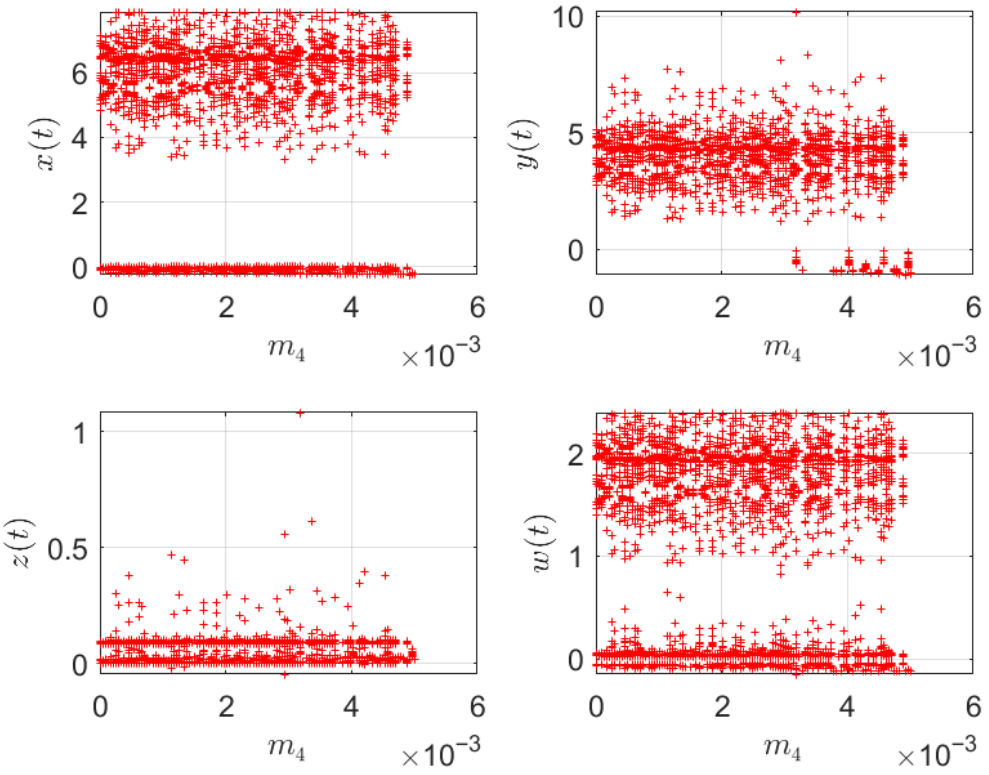

Figure 21. Bifurcation diagrams of $x(t)$, $y(t)$, $z(t)$, and $w(t)$ with respect to m_4. Even small m_4 values induce chaotic motion.

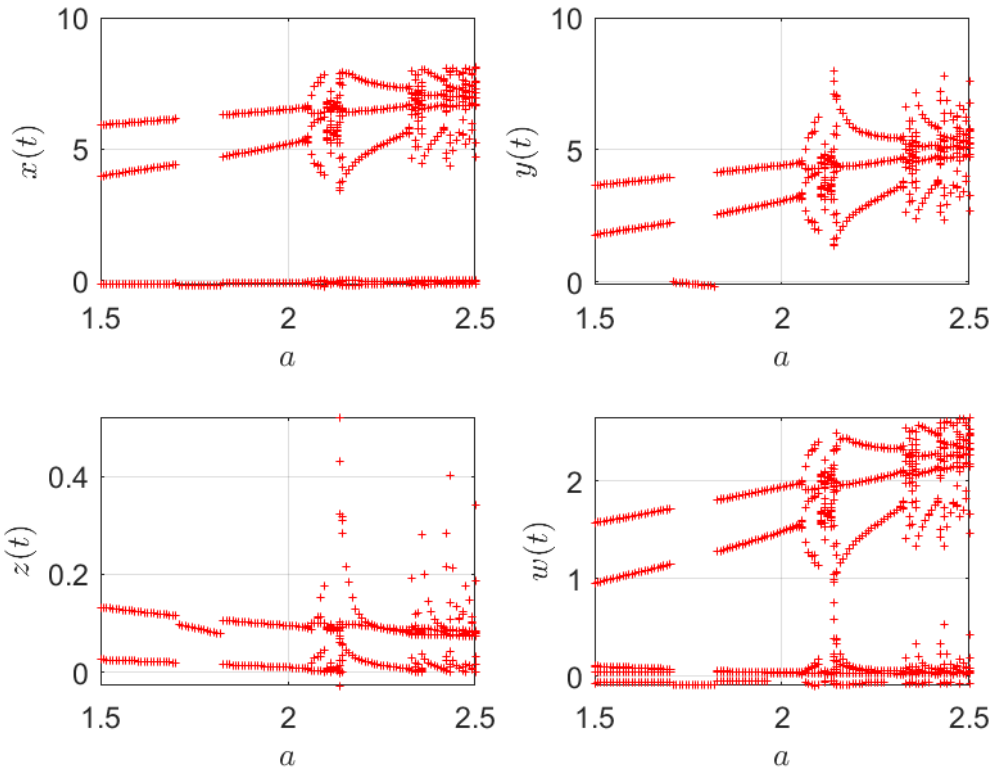

Figure 22. Bifurcation diagrams of $x(t)$, $y(t)$, $z(t)$, and $w(t)$ with respect to a.

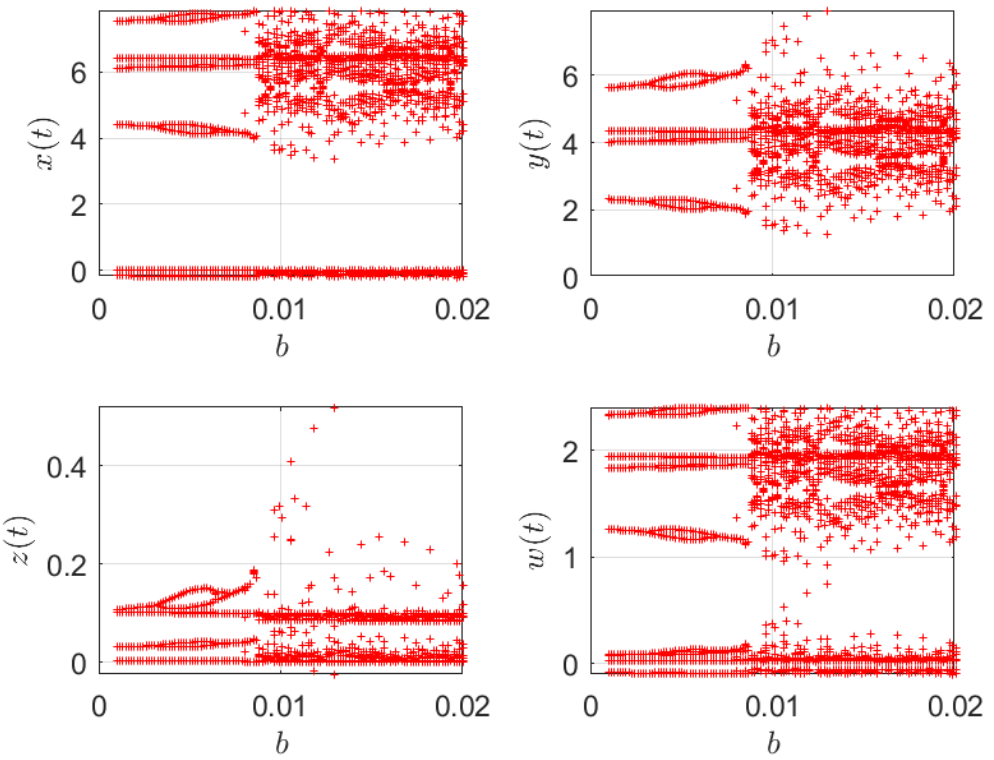

Figure 23. Bifurcation diagrams of $x(t)$, $y(t)$, $z(t)$, and $w(t)$ with respect to b.

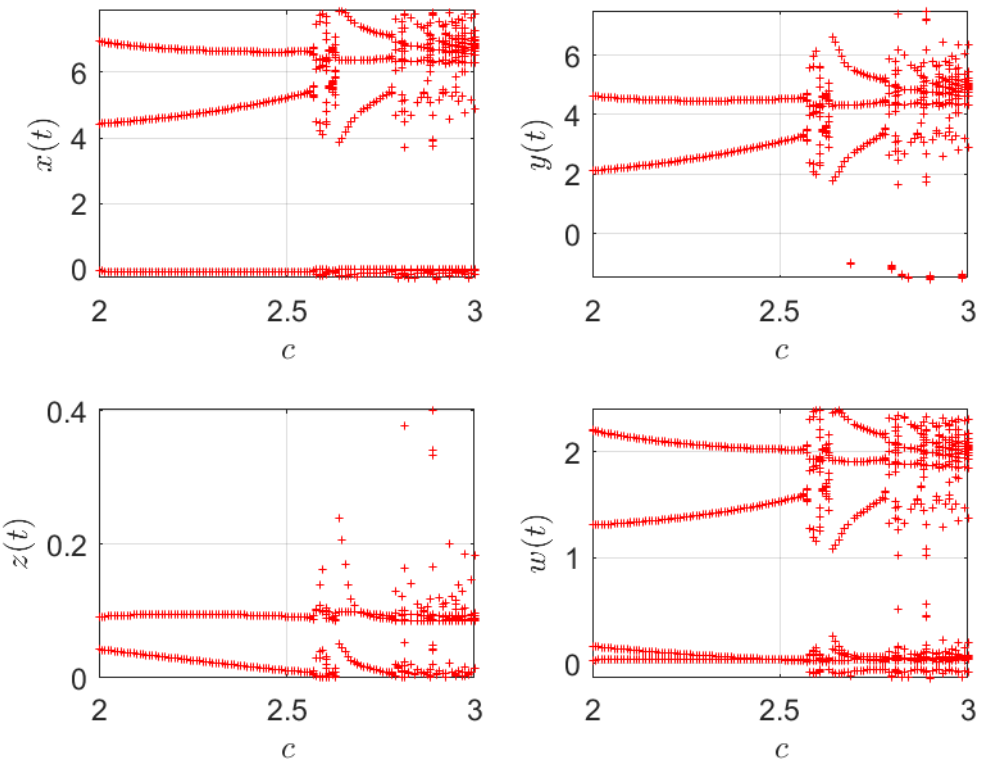

Figure 24. Bifurcation diagrams of $x(t)$, $y(t)$, $z(t)$, and $w(t)$ with respect to c.

3.5. Special Case Analysis of the Financial Model

To better understand the structure and dynamics of the proposed four-dimensional financial system, we consider several special cases by fixing one or more variables or initial conditions. Each case yields a reduced system that provides insight into specific economic scenarios.

Figure 25 presents the state trajectories of the system variables under six distinct special cases.

Case 1: $w = 0$ (No Market Confidence Influence). Setting $w(t) \equiv 0$ reduces the system to

$$\begin{cases} \dot{x} = z + (y - a)x, \\ \dot{y} = 1 - by - x^2, \\ \dot{z} = -x - cz. \end{cases}$$

This corresponds to the classical Ma–Chen system without sentiment effects. The variables $x(t)$, $y(t)$, and $z(t)$ exhibit bounded oscillations and retain long-term stability. Economically, this represents a market driven solely by fundamental relationships between interest rates, investment demand, and price levels, with no influence from investor sentiment—a purely rational-expectations scenario.

Case 2: $x = 0$ (Frozen Interest Rate). Fixing the interest rate gives

$$\begin{cases} \dot{y} = 1 - by + m_2 w, \\ \dot{z} = -cz + m_3 w, \\ \dot{w} = m_4 w. \end{cases}$$

In this scenario, $w(t)$ evolves exponentially, driving $y(t)$ and $z(t)$ upward without the moderating influence of interest rate adjustments. This is analogous to a fixed-monetary-policy regime during which credit expansion or inflation accelerates unchecked, resembling historical episodes where prolonged low interest rates contributed to asset bubbles.

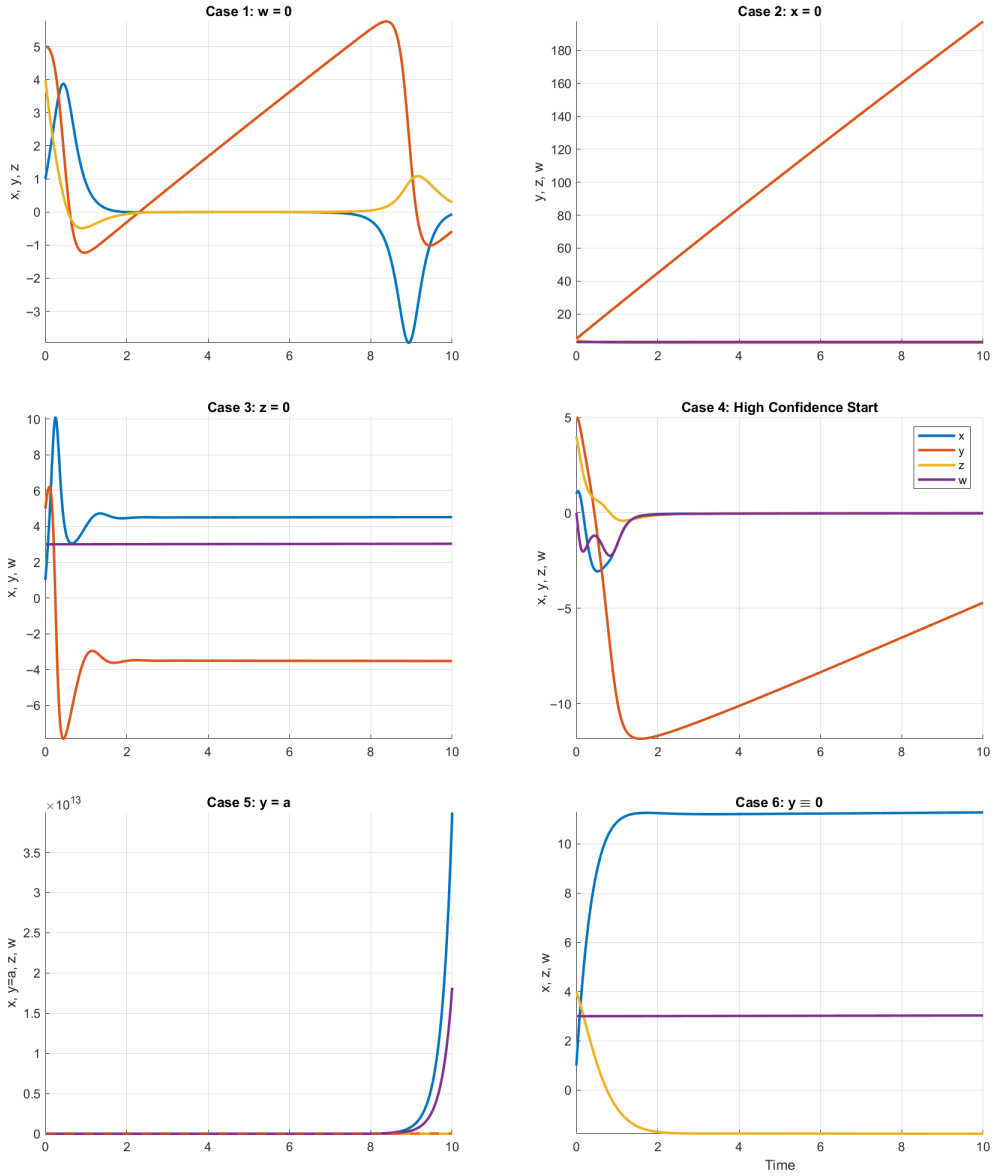

Figure 25. State trajectories for all six special cases of the financial system.

Case 3: $z = 0$ (Frozen Price Index). Assuming a constant price index yields

$$\begin{cases} \dot{x} = (y - a)x + m_1 w, \\ \dot{y} = 1 - by - x^2 + m_2 w, \\ \dot{w} = m_4 w. \end{cases}$$

Here, inflationary effects are absent, and the remaining variables display damped nonlinear oscillations. This reflects an idealised economy with perfectly stable prices, where market adjustments occur through changes in interest rates and investment demand. Such conditions are rare in practice but can be compared to periods of price stability under effective inflation targeting.

Case 4: Large Initial w (Highly Confident Market). To examine the impact of extremely high market confidence, we simulate the full system (2) with a large initial value $w(0) \gg 1$. The initial surge in confidence temporarily boosts $x(t)$, $y(t)$, and $z(t)$, but due to the small m_4 value, the system eventually returns to bounded oscillations. Economically, this reflects

periods such as the peak of the dot-com bubble, where extreme optimism drove rapid market expansion before stabilising forces moderated growth.

Case 5: $y = a$ (Neutral Investment Threshold). Fixing $y(t) \equiv a$ gives the reduced system

$$\begin{cases} \dot{x} = z + m_1 w, \\ \dot{z} = -x - cz + m_3 w, \\ \dot{w} = -axz + m_4 w. \end{cases}$$

Removing the dynamic feedback from investment demand disrupts stability, leading to unbounded growth in $x(t)$ and $z(t)$. This scenario is analogous to credit booms or asset price bubbles where monetary and price variables escalate without corresponding productive investment, often precipitating systemic crises.

Case 6: $y = 0$ (No Investment Demand). Assuming zero investment demand yields

$$\begin{cases} \dot{x} = z - ax + m_1 w, \\ \dot{z} = -x - cz + m_3 w, \\ \dot{w} = m_4 w. \end{cases}$$

Here, $w(t)$ evolves exponentially, with $m_4 > 0$ producing sustained growth in confidence independent of real economic activity. This can destabilise the interest rate and price index through w's coupling, despite the absence of productive investment. Such dynamics resemble stagflationary episodes, where high inflation and interest rates persist even during stagnant or contracting economic output.

In summary, Cases 1 and 3 are dynamically stable; Cases 2, 4, and 6 show sharp but bounded reactions; and Case 5 exhibits chaotic divergence. These results reveal the delicate interplay between interest rate, investment, inflation, and confidence in generating macroeconomic stability.

3.6. Empirical Illustration of a Self-Reinforcing Sentiment Loop

To complement the model-based analysis, we provide a compact empirical illustration using U.S. monthly data: the University of Michigan Consumer Sentiment Index (UMCSENT) and the S&P 500 index (SP500). Daily SP500 observations were averaged to month-end; both series were standardised to zero mean and unit variance (z–scores) to ease comparison.

Figure 26a overlays the two standardised series. Co-movement is evident around large episodes (rallies and drawdowns), while some intervals show divergence (e.g., rising prices alongside deteriorating sentiment). These patterns already suggest a dynamic two-way relation rather than a single leading indicator.

Figure 26b plots the phase trajectory (price on the vertical axis vs. sentiment on the horizontal axis) with one-step arrows. The trajectory forms local loops during pronounced episodes, which is characteristic of feedback: optimism and price appreciation reinforce each other in upswings, whereas pessimism and price declines reinforce each other in downswings.

Figure 26c estimates a reduced-form sentiment map $w_{t+1} = f(w_t)$ via a cubic fit. The fitted curve lies above the 45° line for moderately positive w_t and below it for moderately negative w_t, indicating local regions where deviations tend to persist in the same direction. Intersections with the 45° line mark fixed points; the central crossing corresponds to a locally weakly stable region, whereas the curvature in the shoulders suggests amplification when the system is away from the centre. This pattern mirrors the self-feedback nonlinearity in our model.

Finally, Figure 26d reports lead–lag correlations $\mathrm{Corr}(w_t, z_{t+k})$ for $k \in [-12, 12]$ months, where w_t denotes sentiment and z_t denotes price (both as z–scores). The cross-correlogram is asymmetric: correlations are positive for $k > 0$ with a peak around $k \approx 5$–8 months (price follows sentiment), and mostly negative for $k < 0$ (price movements precede opposite-signed adjustments in sentiment). This asymmetry is consistent with a reflexive loop in which sentiment tends to lead medium-term price dynamics, while large prior price moves can subsequently weigh on household sentiment (e.g., via inflation or macro news). We emphasise that these are associations rather than causal estimates; nonetheless, the directionality is informative for the mechanism.

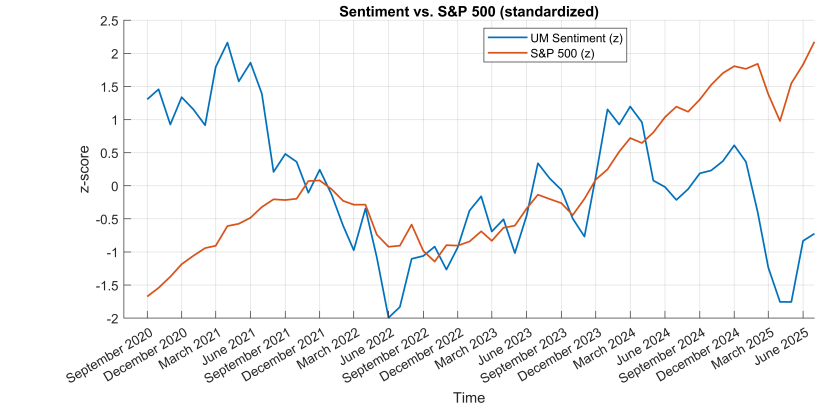

(**a**) Standardised series

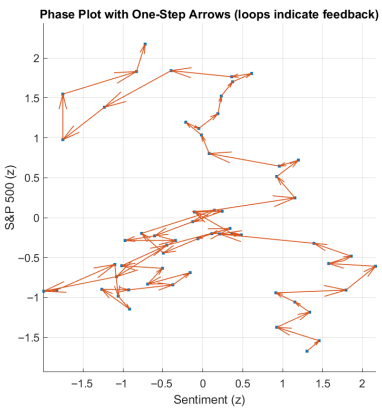

(**b**) Phase plot with arrows

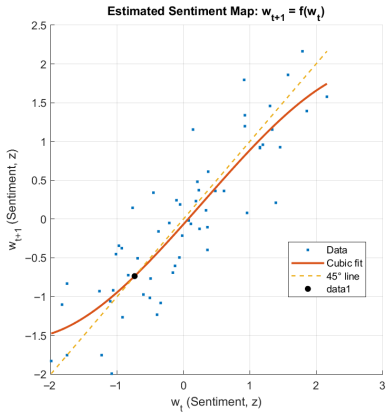

(**c**) Sentiment map

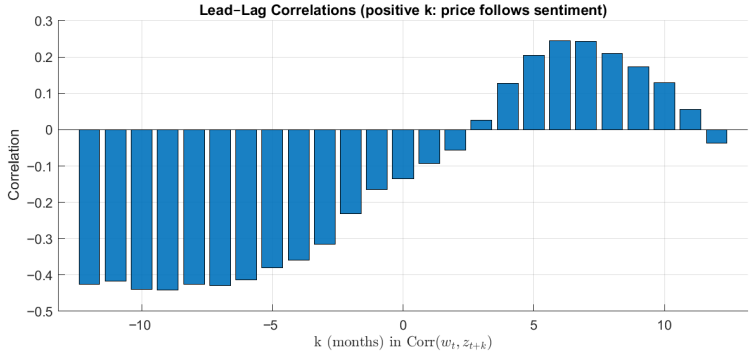

(**d**) Lead–lag correlations

Figure 26. Empirical illustration of a reflexive sentiment–price loop.

Overall, the four panels portray a coherent picture: noticeable co-movement in levels, looped phase trajectories during episodes, sentiment leading prices at medium horizons with an asymmetric cross-correlogram, and a nonlinear persistence map for sentiment. While not

a causal test, these stylised facts are consistent with the model's self-reinforcing confidence channel and justify our focus on diagnostics that capture persistence and amplification.

4. Discussion

Diagnostics consistently indicate low-dimensional chaos. The largest Lyapunov exponent is positive while the sum of exponents is negative (dissipative flow). The Kaplan–Yorke dimension varies non-monotonically within a narrow band (well below the system dimension), pointing to strange attractors with, at most, one positive exponent (chaotic). Broadband power spectra, multistrip Poincaré sections, and rapid separation of nearby trajectories corroborate sensitivity to initial conditions. The results show that the reflexive (confidence) channel has a clear, parameter-sensitive influence: it systematically shifts bifurcation onsets and accentuates intermittent windows in specific regions, while global chaos diagnostics (largest Lyapunov exponent and D_{L}) remain robust across broad settings.

Equilibria obtained under the scanned configurations are dynamically unstable, so trajectories do not settle to steady states; reflexive confidence feedback sustains oscillatory/chaotic motion. Parameter scans reveal period-doubling cascades with intermittent periodic windows. Confidence-related gains govern the onset and width of chaotic bands, while structural parameters shift thresholds; the strength of chaotic signatures is variable across state components, underscoring the need for a multivariate assessment rather than reliance on a single observable.

Special cases further clarify mechanism: fixing confidence or prices yields bounded dynamics, whereas fixing interest or suppressing investment, imposing large initial confidence, or enforcing neutral investment conditions can trigger explosive or chaotic responses. Overall, reflexive feedback reshapes long-run behaviour and acts as a destabilising amplifier, pushing the system into low-dimensional chaotic regimes under modest gains.

5. Conclusions

The reflexive extension produces a dissipative yet chaotic regime with no stable equilibria across broad parameter sets. Chaos is low-dimensional (one positive Lyapunov exponent) and is governed primarily by confidence gains and their coupling to real activity, while structural parameters shift critical thresholds. Evidence includes a positive largest Lyapunov exponent, a non-monotonic Kaplan–Yorke dimension well below the system dimension, unstable equilibria that preclude steady states, and parameter-induced transitions via period-doubling interlaced with periodic windows. The strength of chaotic signatures differs across state variables, underscoring the need for multivariate diagnostics rather than reliance on a single observable.

In our framework, volatility is interpreted in the dynamical sense: it manifests as irregular and aperiodic fluctuations in the interest rate, investment demand, and price index, driven by reflexive market confidence. This behaviour is quantified statistically by a positive largest Lyapunov exponent and supported by bifurcation diagrams showing alternating chaotic and periodic regimes. Hence, the model demonstrates that sentiment-driven feedback not only destabilises equilibria but also sustains volatility as an inherent feature of the system.

As an external validity check, the UMCSENT–S&P 500 pair exhibits looped phase paths and an asymmetric cross-correlogram with sentiment leading prices at 6–8 months; a cubic fit of w_{t+1} on w_t shows curvature consistent with local persistence. These stylised facts align with the model's self-reinforcing confidence channel. The exercise is illustrative rather than causal, but it supports the mechanism we analyse theoretically.

For practical use and further study, control or feedback-damping strategies should be designed to suppress chaotic volatility under targeted conditions; extensions to stochastic or fractional-order dynamics may capture additional real-world features. From a policy

perspective, chaotic windows expand when reflexive gains and investment–confidence coupling are high; measures that damp reflexivity (transparent, rules-based guidance; volatility breaks) and weaken the optimism–investment loop (countercyclical buffers, LTV/DTI and margin limits, leverage/liquidity rules) shift dynamics toward periodic or quasi-periodic regimes without materially altering long-run levels, acting on feedback gains rather than state magnitudes.

Future work will develop and benchmark a neural–fuzzy controller, and assess robustness to disturbances, measurement noise, and parameter drift. We will also examine integrability and possible invariants. In addition, we will study a fractional-order formulation, establish stability with fractional Lyapunov and Mittag–Leffler tools, implement L1 and Grünwald–Letnikov time-stepping schemes, and compare dynamics and control performance with the integer–order model.

Author Contributions: Conceptualisation, U.P.; methodology, U.P. and C.D.; software, U.P. and C.D.; validation, U.P. and C.D.; formal analysis, U.P. and C.D.; investigation, U.P. and C.D.; resources, U.P. and C.D.; data curation, U.P. and C.D.; writing—original draft preparation, C.D.; writing—review and editing, U.P. and C.D.; visualisation, U.P. and C.D.; supervision, U.P.; project administration, U.P. All authors have read and agreed to the published version of the manuscript.

Funding: This research is partially funded by the University of Kelaniya Research Council Grant number RP/03/02/04/02/2025.

Institutional Review Board Statement: Not applicable.

Informed Consent Statement: Not applicable.

Data Availability Statement: The MATLAB (R2019a) code and numerical data used to generate the results in this study are publicly available at the following GitHub repository: https://github.com/upeksha1/finance_system (accessed on 26 October 2025).

Conflicts of Interest: The authors declare no conflicts of interest.

Appendix A. Feasible Parameter Ranges

Figures A1 and A2 report post-transient peak magnitudes of the state variables, $\max_t |x(t)|$, $\max_t |y(t)|$, $\max_t |z(t)|$, and $\max_t |w(t)|$, as each model parameter is varied with all others fixed at the baseline in (3). For each run, the first 80% of the trajectory is discarded as transient; an integration is flagged as divergent if $\|[x, y, z, w]\|_2$ exceeds the preset threshold (black "$\times$" marks on the horizontal axis).

We call a parameter value *feasible* if the integration finishes without divergence and the steady-state peaks remain within numerically moderate bounds (i.e., no order-of-magnitude spikes in the log–scale plots). Applying this conservative criterion yields the workable subranges in Table A1. The intervals intentionally avoid narrow spike windows visible in the scans; other values may still be usable with different initial conditions or tighter solver tolerances.

Table A1. Feasible parameter ranges implied by Figures A1 and A2 (subset of the prior ranges in Table 1).

Parameter	Feasible Range
m_1	$[6, 10]$
m_2	$[4, 8]$
m_3	$[1.0, 2.6]$
m_4	$[0, 5 \times 10^{-3}]$
a	$[1.5, 2.5]$
b	$[0.0, 0.2]$
c	$[2, 3]$

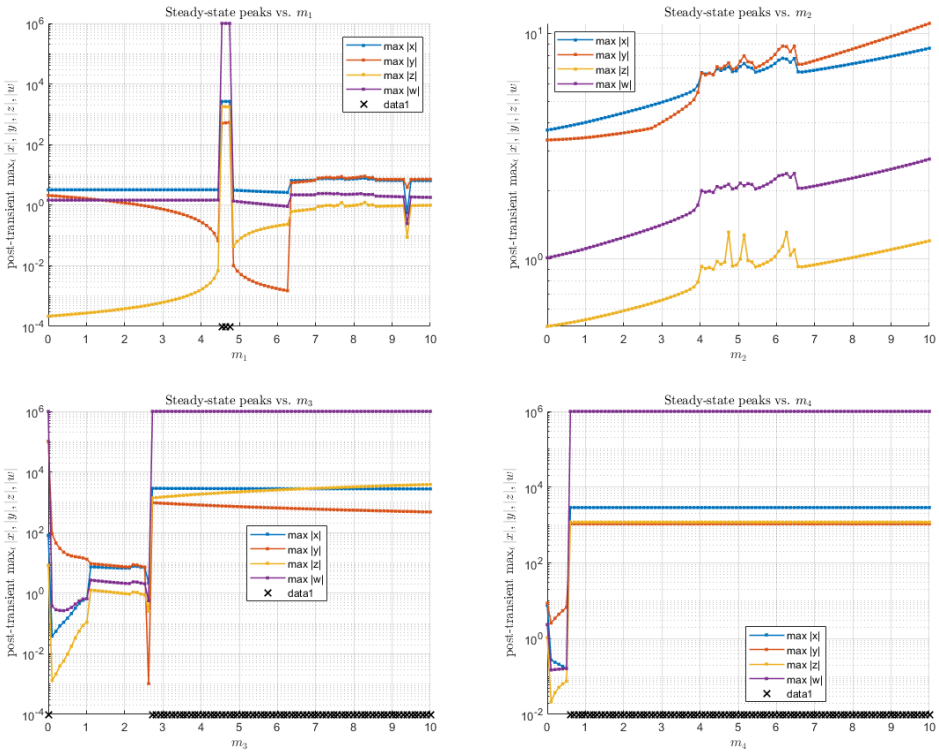

Figure A1. Amplitude scans for confidence-related parameters. Each line shows the post-transient peak of $|x|$, $|y|$, $|z|$, or $|w|$ at each grid point. Crosses (when present) mark early termination due to divergence.

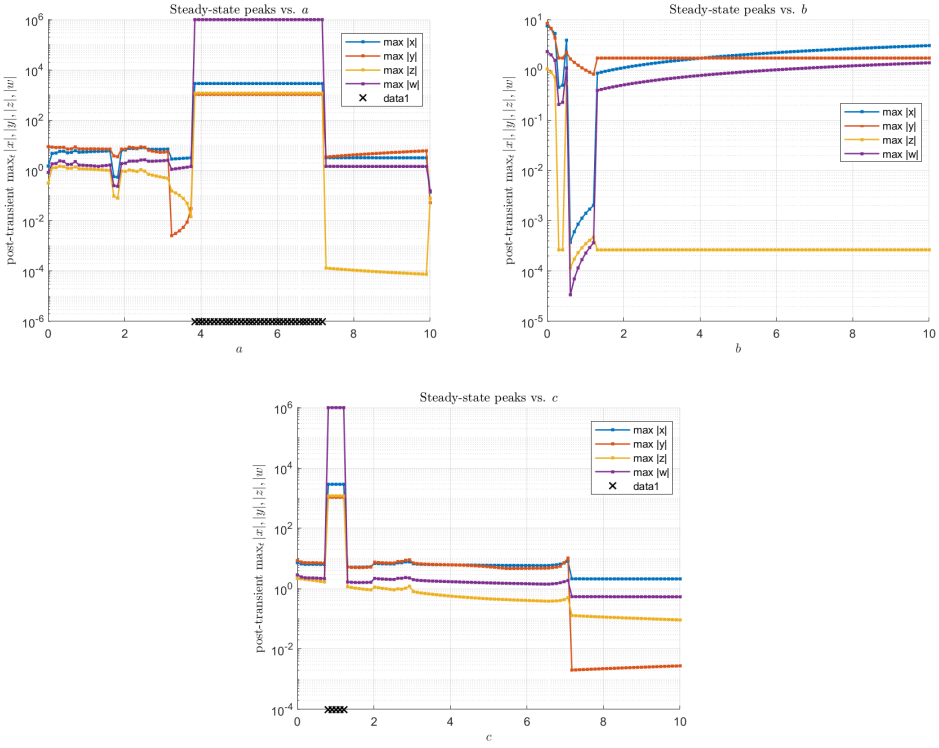

Figure A2. Amplitude scans for structural parameters.

These intervals agree with the economic ranges in Table 1. For the reflexivity coefficient in particular, we adopt the conservative $m_4 \leq 5 \times 10^{-3}$ bound used in the simulations to avoid blow-up, which still lies comfortably inside the broader economically plausible range.

References

1. Grandmont, J.M. On Endogenous Competitive Business Cycles. *Econometrica* **1985**, *53*, 995–1045. [CrossRef]
2. Brock, W.A.; Hommes, C.H. A Rational Route to Randomness. *Econometrica* **1997**, *65*, 1059–1095. [CrossRef]
3. Hommes, C.H. Heterogeneous Agent Models in Economics and Finance. In *Handbook of Computational Economics*; Judd, K.L., Tesfatsion, L., Eds.; Elsevier: Amsterdam, The Netherlands, 2006; Volume 2, pp. 1109–1186.
4. Zhang, W.B. *Discrete Dynamical Systems, Bifurcations and Chaos in Economics*; Elsevier: Amsterdam, The Netherlands, 2006; Volume 204.
5. Foroni, I.; Gardini, L. Homoclinic bifurcations in heterogeneous market models. *Chaos Solitons Fractals* **2003**, *15*, 743–760. [CrossRef]
6. Mihailescu, E. Inverse limits and statistical properties for chaotic implicitly defined economic models. *J. Math. Anal. Appl.* **2012**, *394*, 517–528. [CrossRef]
7. Ma, J.H.; Chen, Y.S. Study for the Bifurcation Topological Structure and the Global Complicated Character of a Kind of Non-linear Finance System (I). *Appl. Math. Mech.* **2001**, *22*, 1119–1128.
8. Ma, J.H.; Chen, Y.S. Study for the Bifurcation Topological Structure and the Global Complicated Character of a Kind of Non-linear Finance System (II). *Appl. Math. Mech.* **2001**, *22*, 1236–1242.
9. Xin, B.; Zhang, Q. Finite-Time Stability Analysis and Control Synthesis for a Financial System with Market Confidence. *Nonlinear Dyn.* **2015**, *80*, 1721–1731.
10. Soros, G. Fallibility, reflexivity, and the human uncertainty principle. *J. Econ. Methodol.* **2013**, *20*, 309–329. [CrossRef]
11. Filimonov, V.; Sornette, D. Quantifying Reflexivity in Financial Markets: Toward a Prediction of Flash Crashes. *Phys. Rev. E* **2012**, *85*, 056108. [CrossRef] [PubMed]
12. Greenwood, R.; Hanson, S.G.; Jin, L.J. *Reflexivity in Credit Markets*; NBER Working Paper 25747; National Bureau of Economic Research: Cambridge, MA, USA, 2019. [CrossRef]
13. Wyart, M.; Bouchaud, J.P. Self-Referential Behaviour, Overreaction and Conventions in Financial Markets. *J. Econ. Behav. Organ.* **2003**, *63*, 1–24. [CrossRef]
14. Xin, B.; Zhang, J. Finite-time stabilizing a fractional-order chaotic financial system with market confidence. *Nonlinear Dyn.* **2015**, *79*, 1399–1409. [CrossRef]
15. Akerlof, G.A.; Shiller, R.J. *Animal Spirits: How Human Psychology Drives the Economy, and Why It Matters for Global Capitalism*; Princeton University Press: Princeton, NJ, USA, 2009.
16. Barsky, R.B.; Sims, E.R. Information, Animal Spirits, and the Meaning of Consumer Confidence. *Am. Econ. Rev.* **2012**, *102*, 1343–1377. [CrossRef]
17. Bloom, N. The Impact of Uncertainty Shocks. *Econometrica* **2009**, *77*, 623–685. [CrossRef]
18. Gennaioli, N.; Ma, Y.; Shleifer, A. Expectations and Investment. *J. Financ. Econ.* **2016**, *122*, 195–214. [CrossRef]
19. Shiller, R.J. Why Do People Dislike Inflation? In *NBER Macroeconomics Annual 1997*; Bernanke, B.S., Rotemberg, J.J., Eds.; MIT Press: Cambridge, MA, USA, 1997; pp. 159–218.
20. Mankiw, N.G.; Reis, R. Sticky Information versus Sticky Prices: A Proposal to Replace the New Keynesian Phillips Curve. *Q. J. Econ.* **2002**, *117*, 1295–1328. [CrossRef]
21. Minsky, H.P. *Stabilizing an Unstable Economy*; McGraw–Hill: Columbus, OH, USA, 1986.
22. Ott, E. *Chaos in Dynamical Systems*, 2nd ed.; Cambridge University Press: Cambridge, UK, 2002. [CrossRef]
23. Kantz, H.; Schreiber, T. *Nonlinear Time Series Analysis*, 2nd ed.; Cambridge Nonlinear Science Series; Cambridge University Press: Cambridge, UK, 2004; Volume 7.
24. Kaplan, J.L.; Yorke, J.A. Chaotic Behavior of Multidimensional Difference Equations. In *Functional Differential Equations and Approximation of Fixed Points*; Lecture Notes in Mathematics; Peitgen, H.O., Walter, H.O., Eds.; Springer: Berlin/Heidelberg, Gemrany, 1979; Volume 730, pp. 204–227. [CrossRef]
25. Takens, F. Detecting strange attractors in turbulence. In *Dynamical Systems and Turbulence, Warwick 1980*; Lecture Notes in Mathematics; Rand, D., Young, L.S., Eds.; Springer: Berlin, Heidelberg, 1981; Volume 898, pp. 366–381. [CrossRef]
26. Wolf, A.; Swift, J.B.; Swinney, H.L.; Vastano, J.A. Determining Lyapunov exponents from a time series. *Phys. D Nonlinear Phenom.* **1985**, *16*, 285–317. [CrossRef]
27. Benettin, G.; Galgani, L.; Giorgilli, A.; Strelcyn, J.M. Lyapunov Characteristic Exponents for Smooth Dynamical Systems and for Hamiltonian Systems; A Method for Computing All of Them. Part 1: Theory. *Meccanica* **1980**, *15*, 9–20. [CrossRef]
28. Benettin, G.; Galgani, L.; Giorgilli, A.; Strelcyn, J.M. Lyapunov Characteristic Exponents for Smooth Dynamical Systems and for Hamiltonian Systems; A Method for Computing All of Them. Part 2: Numerical Application. *Meccanica* **1980**, *15*, 21–30. [CrossRef]